Genome Biology

RESEARCH

Open Access

Phase separation of β-catenin assembles active loop hubs in colorectal cancer

Jiyuan Yang[1†], Jun Sun[2,3†], Hanyi Zhang[1,4†], Yangyinhui Yu[5†], Feng Chen[1], Jingyun Mo[1], Susu Luo[1], Yang Xu[1], Linfeng Zhong[1], Delin Tan[6], Yingnan Lin[1], Yujia Liao[1], Yujia Zhang[1], Jiaxiu Zhang[1], Wanting Chen[1], Xiaona Huang[1], Yan Peng[1], Huabin Gao[7], Huaiming Wang[6], Qing Gong[1*] and Jia Wang[1*]

[†]Jiyuan Yang, Jun Sun, Hanyi Zhang and Yangyinhui Yu contributed equally to this work.

*Correspondence: gongqing@gzhmu.edu.cn; wangjia@gzhmu.edu.cn

[1] GMU-GIBH Joint School of Life Sciences, Guangdong Provincial Key Laboratory of Protein Modification and Disease, The Guangdong-Hong Kong-Macao Joint Laboratory for Cell Fate Regulation and Diseases, Guangzhou Institute of Cancer Research, the Affiliated Cancer Hospital, Guangzhou Medical University, Guangzhou 511436, China
Full list of author information is available at the end of the article

Abstract

Background: Aberrant three-dimensional genome organization is a hallmark of cancer. However, the underlying regulatory mechanisms remain elusive.

Results: Here, we identify β-catenin associated loop hubs in colorectal cancer HCT116 cells using HiChIP profiling. These hubs exhibit an active transcriptional environment marked by elevated gene expression and H3K4me3 enrichment. Disruption of loop hub formation by artificial DNA methylation suppresses hub gene expression and inhibits colorectal cancer growth, indicating its functional importance in cancer. Mechanistically, β-catenin forms phase-separated condensates that are closely associated with loop hubs. By proximity labeling and genomic analyses, we identify and validate the components within β-catenin condensates at loop hubs. We further characterize FUS as a structural scaffold for β-catenin condensate assembly, whereas PARP1 maintains active transcription via H3K4me3. Depletion of either component attenuates condensate function through distinct regulatory mechanisms.

Conclusions: Our findings reveal that β-catenin condensates orchestrate gene regulatory networks by assembling higher-order chromatin architecture, providing new insights into a mechanistic link between phase separation, genome organization and cancer progression.

Keywords: Loop hub, Phase separation, Condensate, Scaffold, β-catenin

Background

Chromatin loop-based transcriptional regulation is critically important for cell fate determination [1–3]. Chromatin loops are mediated by various proteins, and several techniques, such as ChIA-PET, HiChIP and PLAC-seq, have been developed to capture these loops through protein-mediated interactions [4–6]. Aberrant alterations in chromatin looping have been implicated in various cancers [7–9], leading to widespread dysregulation of gene expression. However, tumorigenesis is unlikely to result from the misexpression of a single gene; instead, it arises from the synergistic dysregulation of

multiple genes. To elucidate the mechanisms underlying such coordinated regulation, loop hubs provide an ideal framework, as they physically connect multiple genes to enable their simultaneous regulation [10, 11]. Indeed, the aberrant co-activation of cancer-related genes is thought to be a driving force in carcinogenesis. The formation of loop networks linking these genes is essential for robust co-transcription, making the identification and functional validation of oncogenic loop hubs critical in cancer research.

The formation of multi-loop hubs requires the accumulation of proteins at specific genomic loci [12]. This accumulation often occurs through phase separation, a biophysical process that drives the formation of membraneless condensates [13]. These condensates provide a dynamic and spatially confined environment that facilitates the coordinated regulation of genes within loop hubs. The functional properties of phase-separated condensates are determined by their molecular components. For instance, condensate enriched in MED1 or BRD4 are typically associated with strong transcriptional activation [14, 15], whereas those containing Polycomb proteins are linked to transcriptional repression [16]. Functionally, the proteins within a phase-separated condensate can be classified into two major categories: scaffold proteins, which drive phase separation, and client proteins, which are dispensable for condensate formation but are selectively recruited through interactions with scaffolds [17–19]. Representative scaffold proteins include MED1 in transcriptional activation, SRSF2 in RNA splicing, HP1α in heterochromatin formation, and FIB1 in nucleolar ribosome biosynthesis [18]. In contrast, client molecules are more diverse, encompassing proteins, nucleic acids, metabolites, and ions. Thus, identifying the molecular components of oncogenic phase-separated condensates is essential for understanding how cancer-associated factors regulate chromatin architecture and transcriptional programs.

β-catenin, encoded by the *CTNNB1* gene, is a key factor of the WNT signaling pathway and plays a crucial oncogenic role in colorectal cancer (CRC). Emerging evidence suggests that β-catenin has the potential to undergo phase separation, particularly in association with Mediator condensates [20]. In this study, we employed β-catenin and H3K4me3 HiChIP to identify activate loop hubs in CRC and evaluated their functional significance in tumorigenesis. Furthermore, we investigated the phase separation mechanism underlying loop hub formation. Our findings reveal that β-catenin undergoes phase separation and accumulates at specific genomic loci, forming multi-loop hubs that regulate key cancer-regulatory genes, thereby promoting CRC growth.

Results

Identification of β-catenin-associated loop hubs in HCT116 cells

Transcription factors can directly regulate genome architecture to control gene transcription [12, 21]. To investigate the relationship between cancer-associated factors, genome organization and gene regulatory network in cancer (Fig. 1a), we employed β-catenin HiChIP to identify β-catenin-associated chromatin loops in the CRC cell line HCT116 (Additional file 1: Fig. S1a). These β-catenin-associated loops exhibited several features, including a negative correlation between loop length and both loop quantity and strength (Additional file 1: Fig. S1b, c), and were originally covered by Hi-C across several length scales (Additional file 1: Fig. S1d). To determine whether loops identified in HCT116 cell line were also present in CRC tissues, we compared the reads from

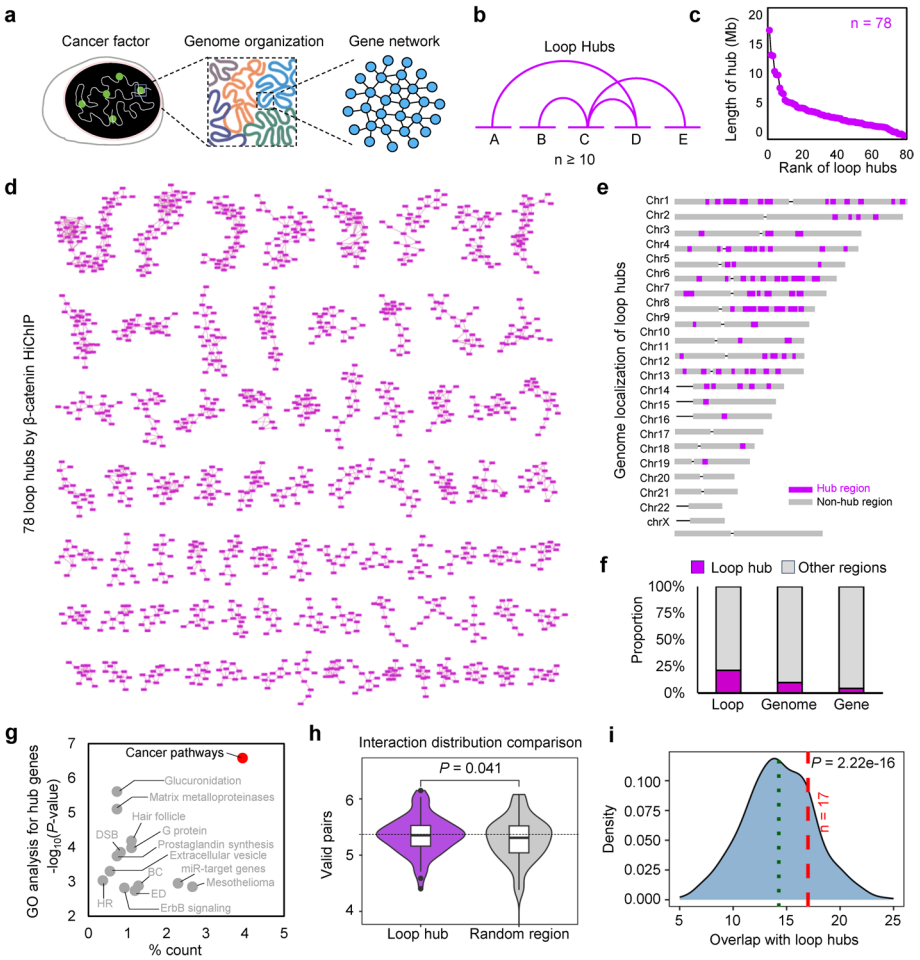

Fig. 1 Identification of Loop Hubs in HCT116 cells. **a** Scheme showing the relationship among cancer factor, genome reorganization and gene regulatory network identified in this study. **b** Chromatin loops identified from HiChIP data are utilized to define loop hubs. Loop hubs are considered as linking many loops together through the targeting genes. That means if two loops have the same targeting gene, these loops are connected. When the total number of genes exceeds 10, we classify these connections as loop hubs. loop hubs indicate genome regions where multiple loops converge, suggesting a higher-order chromatin structure that potentially facilitates coordinated gene regulation. **c** Ranking of the loop hubs ($n = 78$) according to the length of loop hub regions. **d** Cytoscape showing all the 78 β-catenin-associated loop hubs identified by HiChIP. Boxes stand for hub genes while lines represent loops connecting the genes. **e** Genome distribution of the 78 loop hubs. **f** Proportions of loops, genome coverage, and genes within loop hubs to those of whole genome. **g** Functional enrichment analysis of genes in loop hubs. Genes within loop hubs were analyzed using the Metascape network service, revealing enrichment in cancer-related pathways. This suggests that genes in these hubs may play crucial roles in tumorigenesis and cancer progression. **h** Violin diagram showing the distribution of the Hi-C valid pairs of CRC tissues in loop hubs and random regions. **i** Numbers of loop hubs identified in CRC tissues overlapping with the β-catenin-associated loop hubs in HCT116 cells ($n = 17$, red dotted line) compared to a null distribution consisting of 1,000 draws of randomly selected regions (mean = 14.27, green dotted line)

HCT116 cells with those from normal colon and CRC tissues [22]. We found that reads from the HCT116 cell line were more highly correlated with those from CRC tissues than normal colon tissues (Additional file 1: Fig. S1e). Moreover, direct comparison of the reads revealed a strong correlation between HCT116 cells and CRC tissues (Additional

file 1: Fig. S1f). These results indicate that the loops identified in the HCT116 cell line are more similar to those detected in CRC tissues.

To further characterize the structural organization of these loops, we identified loop hubs as genomic structures in which at least 10 genes are interconnected through a loop network (Fig. 1b). Using this criterion, we identified a total of 78 loop hubs in HCT116 cells (Fig. 1c, d), which span megabase-scale genomic regions (Fig. 1c). The loop hubs exhibited nonrandom genomic distribution, with enrichment on chromosomes 1, 4, 6, 7, 8 and 12, and absence on chromosomes 16, 19, 20, 21 and 22 (Fig. 1e). These loop hubs accounted for approximately one quarter of all loops, covered 10% of the genome, but interconnected only 4.3% of genes (Fig. 1f), indicating the transcription apparatus may be concentrated for important gene regulation. Gene Ontology (GO) analysis showed that the genes within the loop hubs were significantly enriched in cancer-related pathways (Fig. 1g), highlighting the potential importance of these structures in CRC. To assess whether loop hubs identified in the HCT116 cell line were also present in CRC tissues, we compared the enrichment of Hi-C valid pairs between loop hubs and randomly selected genomic regions. We found that the Hi-C valid pairs derived from CRC tissues were significantly enriched in loop hub regions compared to randomly selected genomic regions (Fig. 1h and Additional file 1: Fig. S1g). Moreover, loop hubs identified in CRC tissues were significantly correlated with the genomic regions covering loop hubs identified in HCT116 cells compared to randomly selected genomic regions (Fig. 1i). Furthermore, loop hubs in HCT116 cells showed a higher overlap with loop hubs in CRC tissues than with those in normal colon tissues ($n = 17$ vs $n = 5$, Fig. 1i and Additional file 1: Fig. S1h). Together, these results demonstrate that loop hubs identified in HCT116 cell line are more likely to be present in CRC tissues.

Active transcriptional environment within β-catenin-associated loop hubs

To identify the internal feature of the β-catenin-associated loop hubs, we analyzed gene expression using RNA-seq. We observed that genes within loop hubs exhibited higher expression levels than those outside the hubs (Fig. 2a). Moreover, the loop hub genes displayed elevated expression in HCT116 cells compared with the same genes in normal colon epithelial cells (Fig. 2b and Additional file 2: Table S1), suggesting that loop hubs create a cancer-specific transcriptional activation environment.

Next, we investigated the effect of Wnt/β-catenin signaling on gene expression within loop hubs. β-catenin depletion led to marked change in gene expression [23], with more upregulated than downregulated differentially expressed genes (DEGs) (2298 vs 1591, Additional file 1: Fig. S2a). This result indicates that β-catenin has dual roles in activating and repressing gene expression, with the repressive effect being more pronounced. Notably, upon β-catenin deletion, the proportion of downregulated DEGs among the 476 expressed loop hub genes was markedly higher than both the proportion of upregulated DEGs within loop hubs (Fig. 2c, d), and the proportion of downregulated DEGs among 476 randomly selected genes (Fig. 2d-g and Additional file 1: Fig. S2b), revealing that β-catenin mainly supports gene transcription within loop hubs. Furthermore, when Wnt signaling was activated by CHIR99021 treatment [24], the proportions of both upregulated genes and upregulated DEGs within loop hubs were significantly higher

than those of randomly selected genes (Fig. 2h-j). These results demonstrate that Wnt/β-catenin signaling positively regulates the expression of loop hub genes.

To further validate the active transcriptional environment within loop hubs, we generated H3K4me3-associated loops using HiChIP, as this epigenetic modification is a marker of gene activation. A subset of H3K4me3 loops overlapped with β-catenin loops genome-wide in HCT116 cells (Fig. 2k, l). Intriguingly, the percentage of the overlapping loops in loop hub regions is markedly higher than that of either H3K4me3-specific loops or β-catenin-specific loops (Fig. 2m). Moreover, the overlap rate between H3K4me3 loops and β-catenin loops increased from 35 to 51% when analyses were restricted to loop hub regions (Fig. 2n). These results reveal that the loop hub regions are more transcriptionally active than other genomic regions. Furthermore, we generated the active loop hubs by jointly considering both β-catenin and H3K4me3 loops (Additional file 1: Fig. S2c and Additional file 3: Table S2). Genes within the active loop hubs largely overlapped with those within β-catenin loop hubs (Additional file 1: Fig. S2d). We ranked the active loop hubs according to gene and loop number (Additional file 1: Fig. S2e, f), and selected three representative loop hubs of varying sizes for further functional validation (Fig. 2o-q and Additional file 1: Fig. S2g).

Attenuation of loop hubs by DNA methylation suppresses HCT116 cell growth

To assess the functional importance of the loop hubs in gene expression and CRC growth, we attenuated the structures by elevating DNA methylation levels at loop hubs using the dCas9-KRAB-MeCP2 system (Additional file 1: Fig. S3a, b) [25], as higher DNA methylation level inhibits transcription factor binding and represent an effective strategy to disrupt chromatin loops [7, 8]. Notably, the genomic regions selected for this perturbation were only enriched with loop anchors rather than gene

(See figure on next page.)

Fig. 2 Active Transcription Environment within Loop Hubs. **a** Genes within loop hubs tend to have higher expression levels. RNA-seq data showing the genes within loop hubs exhibit elevated expression compared to genes outside these structures, suggesting that loop hubs may facilitate enhanced transcriptional activity. $P = 0.0027$ by Wilcoxon Test. **b** Loop hub genes in the HCT116 cell line tend to have higher expression levels compared to the NCM460 cell line. Comparative expression analysis indicates that genes in loop hubs are more actively transcribed in CRC HCT116 cells, implying a potential relationship between loop hubs and cancer gene regulation. $P = 0.00044$ by Wilcoxon Test. **c** Venn diagram showing the number of overlapping genes between down- or up-regulated DEGs upon *CTNNB1* deletion and the 476 expressed genes within loop hubs. **d** The relative proportions of down- and up-regulated DEGs of loop hub genes and randomly selected genes with equal numbers. **e**, **f** The proportions of (**e**) downregulated genes and (**f**) downregulated DEGs in loop hubs are significantly higher than those of random genes with equal number in response to CTNNB1 deletion. **g** *CTNNB1* deletion suppresses gene expressions within loop hubs at chromosome 1 locus. **h**, **i** The proportions of (**h**) upregulated genes and (**i**) upregulated DEGs in loop hubs is significantly higher than those of random genes with equal number in response to activation of Wnt signaling by the chemical CHIP99021. **j** Activation of Wnt signaling by the chemical CHIP99021 enhances gene expressions within loop hubs at chromosome 1 locus. **k** Aggregate peak analysis (APA) of the β-catenin- and H3K4me3-associated loops in HCT116 cells. **l** Venn diagram showing 35% of H3K4me3 loops are overlapped with β-catenin genome-wide in HCT116 cell line. Loops are generated using HiChIP data. **m** The percentage of the overlapped loops in loop hub regions is markedly higher than either H3K4me3-specific loops or β-catenin-specific loops. **n** Venn diagram showing the overlapping rate increased to 51% between H3K4me3 loops and β-catenin loops when only considering the loop hub regions. **o** Visualization of β-catenin and H3K4me3 loops in loop hub 1 in HCT116 cell line. HiChIP data reveal the presence and configuration of loops in loop hub 1. **p, q** Demonstration of β-catenin (**p**) and H3K4me3 (**q**) mediated gene interactions in loop hub 1. Red genes indicate those mediated by both β-catenin and H3K4me3 loops

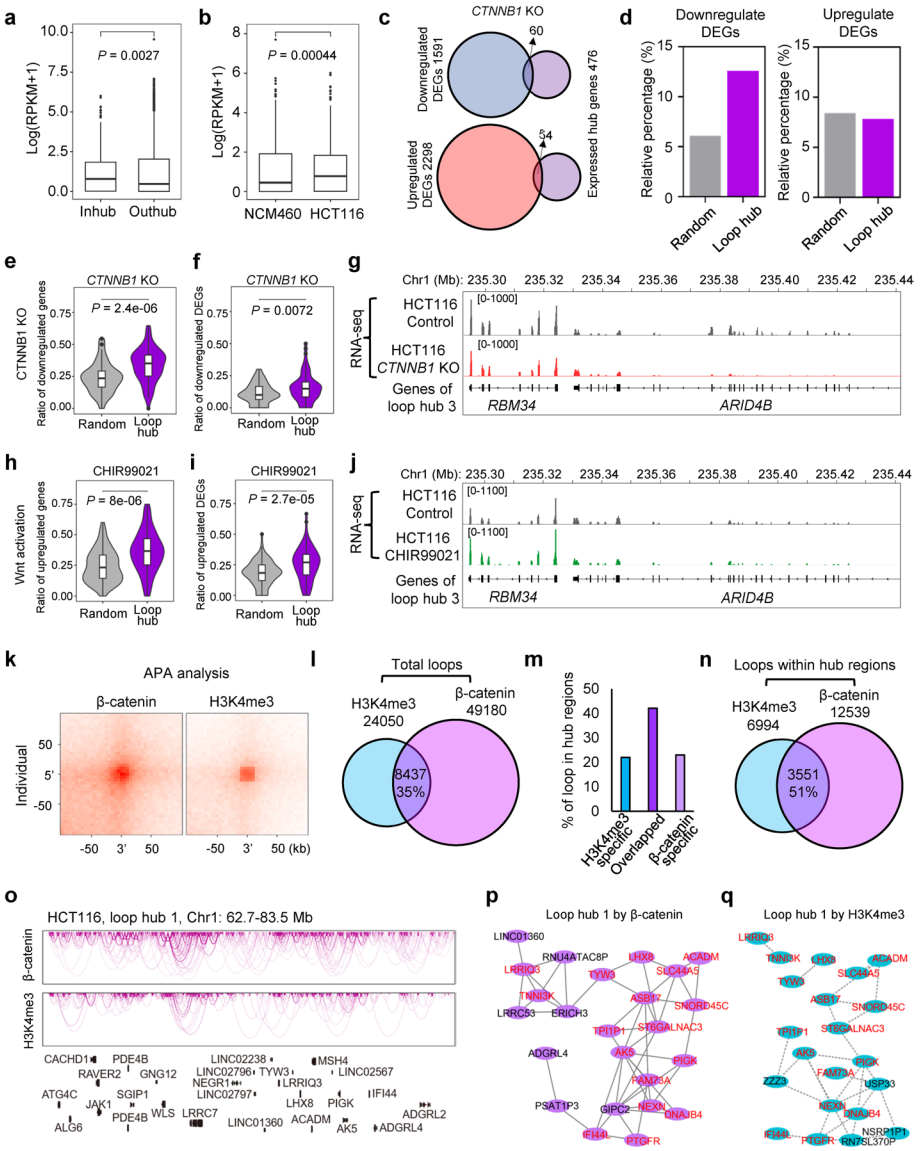

Fig. 2 (See legend on previous page.)

promoters (Fig. 3a, b). This design ensures that loops, rather than genes themselves, are selectively perturbed, thereby allowing potential changes in gene expression to be attributed to loop disruption rather than to artificial DNA methylation. Consequently, this treatment enhanced DNA methylation levels at the CpG sites near the sgRNA-targeted sequence as detected by bisulfite sequencing (Fig. 3c, d), resulting in decreased loop strength within the loop hubs as measured by the quantitative analysis of chromosome conformation capture assays (3C-qPCR, Fig. 3e). Moreover, disruption of loop hubs suppressed the expression of the loop hub genes (Fig. 3f). Functional assays, including CCK-8 cell viability and colony formation, confirmed that HCT116 cell growth was markedly inhibited following the elevation of DNA methylation

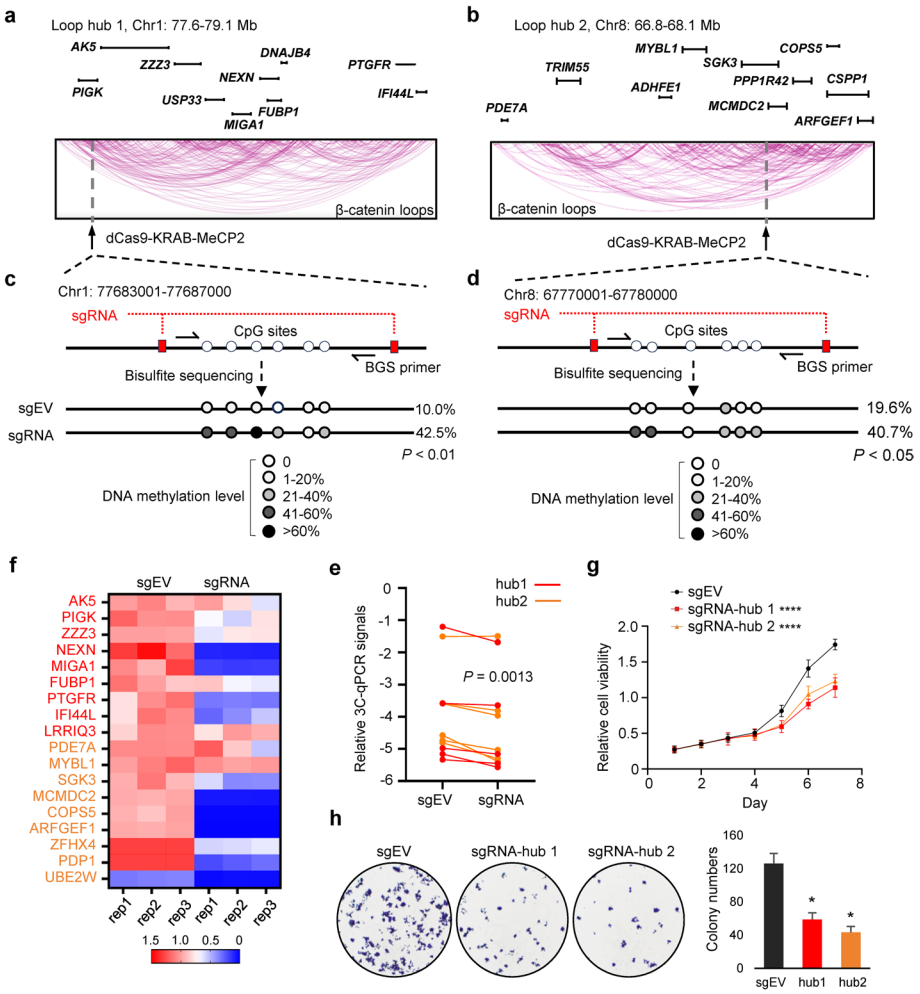

Fig. 3 Induction of DNA methylation at loop hubs suppresses CRC growth. **a**, **b** Scheme depicting the targeting sites of dCas9-KRAB-MeCP2 by sgRNAs at loop hub 1 (**a**) and 2 (**b**), respectively. **c**, **d** Enhanced DNA methylation levels at loop hub 1 (**c**) and 2 (**d**) by dCas9-KRAB-MeCP2 via bisulfite sequencing. The circles represent CpG sites. The color of the circles from white to black represents the methylation level from slight to heavy. **e** 3C-qPCR showing decreased DNA-DNA interactions at loop hub 1 and 2 in response to DNA methylation. Three biological replicates are assayed for 3C-qPCR experiment. **f** Heatmap showing the expression change of the representative genes within loop hub 1 (red) and 2 (orange) by qPCR after induction of DNA methylation by dCas9-KRAB-MeCP2. sgRNA empty vector (sgEV) is used as control. Three biological replicates are assayed for qPCR experiment. **g** Cell viability of the engineering HCT116 cells were determined by CCK8 assay. Values are mean ± SD from three triplicate experiments. ****$P < 0.0001$ compared to control. **h** Representative images and quantification of the colonies formed by the engineering HCT116 cells. Three independent experiments were performed. *$P < 0.05$ compared to control

at loop hubs (Fig. 3g, h). Collectively, these findings underscore the crucial role of β-catenin-associated active loop hubs in supporting CRC cell growth.

Phase separation of β-catenin is associated with loop hubs

As chromatin loops were captured using a β-catenin antibody-based approach [4], we postulated that loop hubs accumulating a high density of loops might be closely associated with the aggregation of β-catenin proteins. Given that phase separation is a

recognized mechanism underlying protein aggregation [13], we hypothesized that β-catenin forms phase-separated condensates localized at loop hub regions.

To test the hypothesis, we first assessed the phase separation capability of β-catenin in vitro, in cell lines and in clinical tissues, respectively. β-catenin contains two short intrinsically disordered regions (IDRs) at its N- and C-termini (Additional file 1: Fig. S4a). We cloned the β-catenin coding sequence into a prokaryotic pET28a vector tagged with eGFP, allowing us to purify the β-catenin–eGFP fusion protein and perform droplet formation assays in vitro (Additional file 1: Fig. S4b). Imaging results revealed that β-catenin forms GFP-positive, micron-sized spherical droplets that move freely in solution. These droplets increased in size with higher β-catenin concentrations and were sensitive to elevated NaCl levels (Fig. 4a, b and Additional file 1: Fig. S4c, d). Moreover, fluorescence recovery after photobleaching (FRAP) demonstrated rapid recovery, confirming the liquid-like properties of the droplets (Fig. 4c, d). However, the droplets of β-catenin were relatively smaller than those formed by several well-known phase-separated proteins under the same conditions [26], indicating that the intrinsic phase separation ability of β-catenin is limited.

Notably, we observed endogenous β-catenin condensates in CRC tissues as well as the HCT116 CRC cell line (Fig. 4e-h), whereas such condensates were not readily detected in normal colon tissues or in the NCM460 normal colon cell line. Moreover, we overexpressed the eGFP-β-catenin in three CRC cell lines, and observed that the exogenous β-catenin formed similar condensates in these cells (Fig. 4i and Additional file 1: Fig. S4e, f), with FRAP analysis again confirming their liquid-like characteristics (Fig. 4j, k). These results support that β-catenin can form condensates with liquid-like behavior in CRC. Furthermore, a combined analysis of SunTag labeling of loop hubs and eGFP-β-catenin fluorescence showed a higher co-localization of β-catenin condensates with loop hubs than with non-loop hub regions (Fig. 4l-o) [27], indicating an association of loop hubs within β-catenin condensates.

Identification of the components of β-catenin condensates at loop hubs

The functional properties of phase separation are determined by the components within the phase-separated condensates. To elucidate how phase separation regulates loop hubs, we applied a dCas9-APEX2-dependent proximity labeling approach in HCT116 cells. This method combines site-specific targeting with simultaneous treatment using biotin-phenol (BP) and hydrogen peroxide (H_2O_2) [28], to biotinylate proteins in the vicinity of target loci. The biotinylated proteins were then enriched using streptavidin-conjugated beads and subsequently identified by mass spectrometry (MS) (Fig. 5a).

For this analysis, we selected three loop hubs for investigation. At each hub, two sgRNAs were designed to target distinct loci (Additional file 1: Fig. S5a and Additional file 4: Table S3). HCT116 cells transfected with dCas9-APEX2 and the appropriate sgRNA were treated with H_2O_2 and BP to induce biotin labeling, while cells not treated with H_2O_2 served as negative controls (Additional file 1: Fig. S5a, b). By subtracting the background proteins from the experimental groups, we generated specific protein pools corresponding to β-catenin condensates at each loop hub. Proteins detected at both sgRNA-targeted loci within each hub were considered positive candidates (Fig. 5b-d and Additional file 1: Fig. S5c-e). The overlap of positive candidates across the three hubs

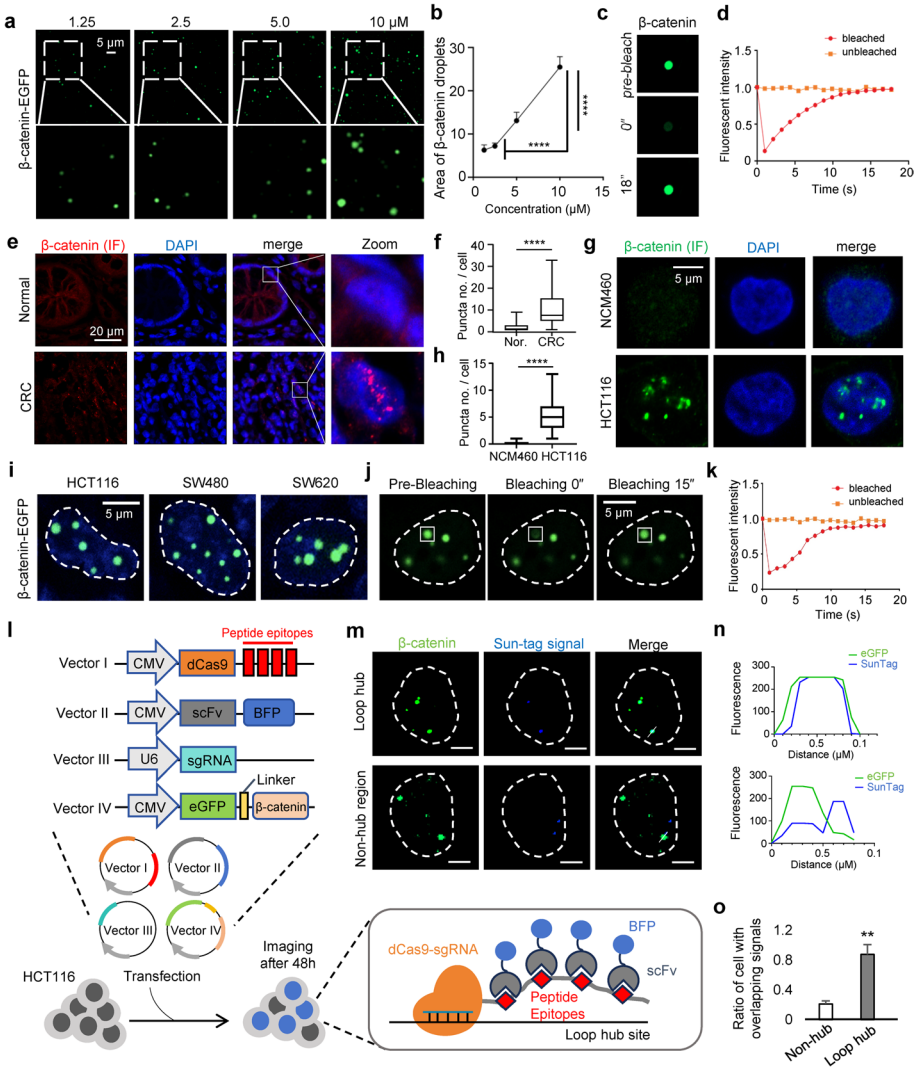

Fig. 4 Co-localization of β-catenin condensates with loop hubs. **a** Representative image showing droplet formation of β-catenin at the indicated concentration in droplet formation buffer with 125 mM NaCl and 10% PEG-8000. **b** Quantification of eGFP-β-catenin droplets with increased concentration in vitro. Values are mean ± SD from three independent experiments. ****$P < 0.0001$. **c** FRAP of β-catenin droplets. Confocal images were taken at indicated time points relative to photobleaching (0). **d** Quantification of FRAP data for eGFP-β-catenin droplets in vitro. **e** Representative images showing the nuclear β-catenin condensates are markedly present in CRC tissues rather than normal colon tissues. Scale bars: 20 μm. **f** Quantification of the nuclear β-catenin condensates between normal colon and CRC tissues. ****$P < 0.0001$. **g** Representative images showing the endogenous β-catenin condensates are markedly present in HCT116 cells rather than NCM460 cells. Scale bars: 5 μm. **h** Quantification of the endogenous β-catenin condensates between NCM460 and HCT116 cells. ****$P < 0.0001$. **i** Representative images showing the exogenous eGFP-β-catenin condensates in three representative CRC cell lines. Scale bars: 5 μm. **j** Representative images of FRAP of eGFP-β-catenin condensates in HCT116 cells. White box highlights the condensates undergoing targeted bleaching. **k** Quantification of FRAP data for eGFP-β-catenin condensates in HCT116 cells. **l** Design of the SunTag experiment. Four vectors carrying dCas9-peptide epitopes, scFv-BFP, sgRNA and eGFP-β-catenin respectively were co-transfected into HCT116 cells. dCas9-peptide epitopes fusion protein targets loop hub site by sgRNA. The four tandem copies of peptide epitope recruit BFP-tagged scFv for amplified blue fluorescence at the site. **m** Representative images showing the co-localization of eGFP-β-catenin condensates (green) with loop hub (blue). **n** Line plots showing the fluorescence intensities of GFP and BFP in the white boxes (top) or along the white dotted line (bottom). **o** Percentage of cells with overlapped GFP and BFP fluorescent signals. Values are mean ± SD from three independent experiments. **$P < 0.01$

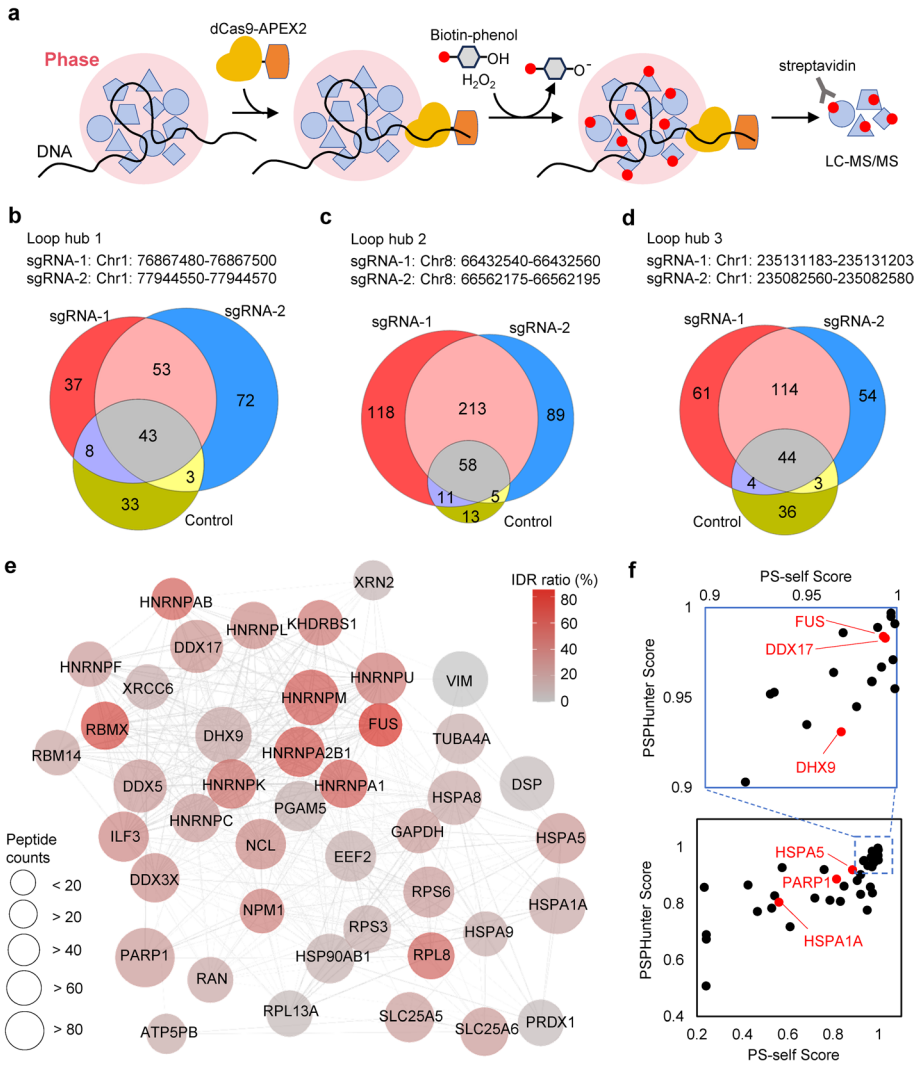

Fig. 5 Identification of the components of β-catenin condensates in CRC. **a** Scheme depicts the process of dCas9-APEX2-dependent proximity labeling for identifying the condensate components at loop hub sites. **b**-**d** Venn diagram showing the numbers of candidate components in condensates at loop hub 1 (**b**), 2 (**c**) and 3 (**d**), respectively. The background proteins (cells treated with BP only) are excluded from the experimental groups (cells treated with both H_2O_2 and BP) to generate the protein pools, respectively. **e** Shared components of β-catenin condensates from three independent experiment targeting the three loop hubs respectively. Deeper color indicates higher IDR ration of the component. Larger circle represents more peptide counts by APEX2-MS. **f** Scatter plot showing the predicted phase separation capacity of each component by PSPHunter (Y axis) and PhaSePred (X axis). Higher score indicates higher potential of phase separation. Enlarged area showing the candidates with both PSPHunter and PhaSePred score more than 0.9. Red dots stand for the candidates for further validation assays

revealed a common set of components associated with β-catenin condensates (Fig. 5e and Additional file 1: Fig. S5f). These components were further ranked based on peptide counts, and potential phase separation ability was assessed by PSPHunter [29], PhaSePred [30], and the ratio of IDR (Fig. 5f and Additional file 1: Fig. S5g, h). From this analysis, PARP1, FUS, HSPA1A, HSPA5, DHX9 and DDX17 were selected as promising candidates for subsequent experimental validation.

Scaffold and client properties of the components in β-catenin condensates

Next, we conducted both in vitro and in vivo experiments to investigate the functional links between the different components. In vitro droplet formation assays revealed that most mCherry-tagged candidates form highly spherical droplets independently, except for PARP1 and DHX9 (Fig. 6a). Upon co-incubation with eGFP-tagged β-catenin, we observed that all these candidate components either fully or partially co-localized with β-catenin droplets (Fig. 6b, c). Notably, PARP1 and DHX9, although unable to form droplets on their own, were accumulated in the droplets of β-catenin (Fig. 6b), suggesting they act as client proteins that are dispensable for droplet formation but can be selectively incorporated. In contrast, droplets formed by HSPA1A and DDX17 showed incomplete co-localization with β-catenin (Fig. 6b), implying that additional cofactors may be necessary for their interaction. Conversely, droplets formed by FUS and HSPA5 were completely co-localized with β-catenin, indicating a strong intrinsic compatibility and suggesting that these components may contribute to the structural assembly of β-catenin condensates. For the in vivo validation, HCT116 cells were co-transfected with vectors encoding mCherry-tagged candidate components and eGFP-tagged β-catenin (Additional file 1: Fig. S6a). Confocal imaging confirmed the co-localization of these components with β-catenin condensates in the nucleus (Additional file 1: Fig. S6b, c). These results validate the presence of the identified components within β-catenin condensates and support the reliability of our component identification using APEX2-dependent proximity labeling.

The limited intrinsic phase separation ability of β-catenin did not hinder β-catenin from forming larger condensates in CRC cells and tissues (Fig. 4e-h), indicating certain proteins may function as scaffolds in vivo to provide structural support and stability to the condensates. Based on the independent droplet-forming ability and complete co-localization with β-catenin, FUS was likely to serve as a scaffold protein. To validate this hypothesis, we mixed β-catenin at increasing concentrations with FUS at fixed concentration (5 μM) in vitro, and evaluated the impact on β-catenin droplets. Intriguingly, FUS facilitated β-catenin droplet formation at lower β-catenin concentrations. As the

(See figure on next page.)

Fig. 6 FUS functions as a scaffold protein of β-catenin condensates at loop hubs. **a** Representative image of droplet formation of the components at 10 μM concentration in droplet formation buffer with 125 mM NaCl and 10% PEG-8000. Scale bar, 5 μm. **b** Representative images showing the co-localization of mCherry-components with eGFP-β-catenin condensates in vitro. Protein concentrations were 10 μM; scale bar, 5 μm. **c** Line plots showing the fluorescence intensities of GFP-β-catenin (green line) and mCherry-components (red line) along the white dotted line. **d** Representative images showing the in vitro droplet formation of β-catenin alone at different concentration, compared with that of β-catenin mixed with 5 μM FUS. Scale bars: 5 μm. **e** Quantification of the mean fluorescence intensity of β-catenin. The data shown are the means ± SD from three independent experiments. $^{****}P < 0.0001$. **f** Numbers of the loop hub genes (red dotted line) overlapping with the targeting genes of β-catenin compared to a null distribution consisting of 10,000 draws of randomly selected genes ($n = 1292$). **g** Numbers of β-catenin peaks (red dotted line) overlapping with loop hubs compared to a null distribution consisting of 10,000 draws of randomly selected genomic regions matching the length of the loop hubs. **h** Venn diagram showing the overlapping between β-catenin and DHX9 peaks identified by ChIP-seq. Green and orange area represent β-catenin specific peaks and shared peaks, respectively. **i** Jaccard similarity showing the shared β-catenin and DHX9 peaks are highly correlated with loop hub genes than β-catenin specific peaks. $^{****}P < 0.0001$. *ns* means no significance. **j** Heatmaps of β-catenin, DHX9 and FUS binding around the TSS regions. **k** ChIP-seq binding profiles for β-catenin, DHX9 and FUS at the loop hub 1 in HCT116 cells

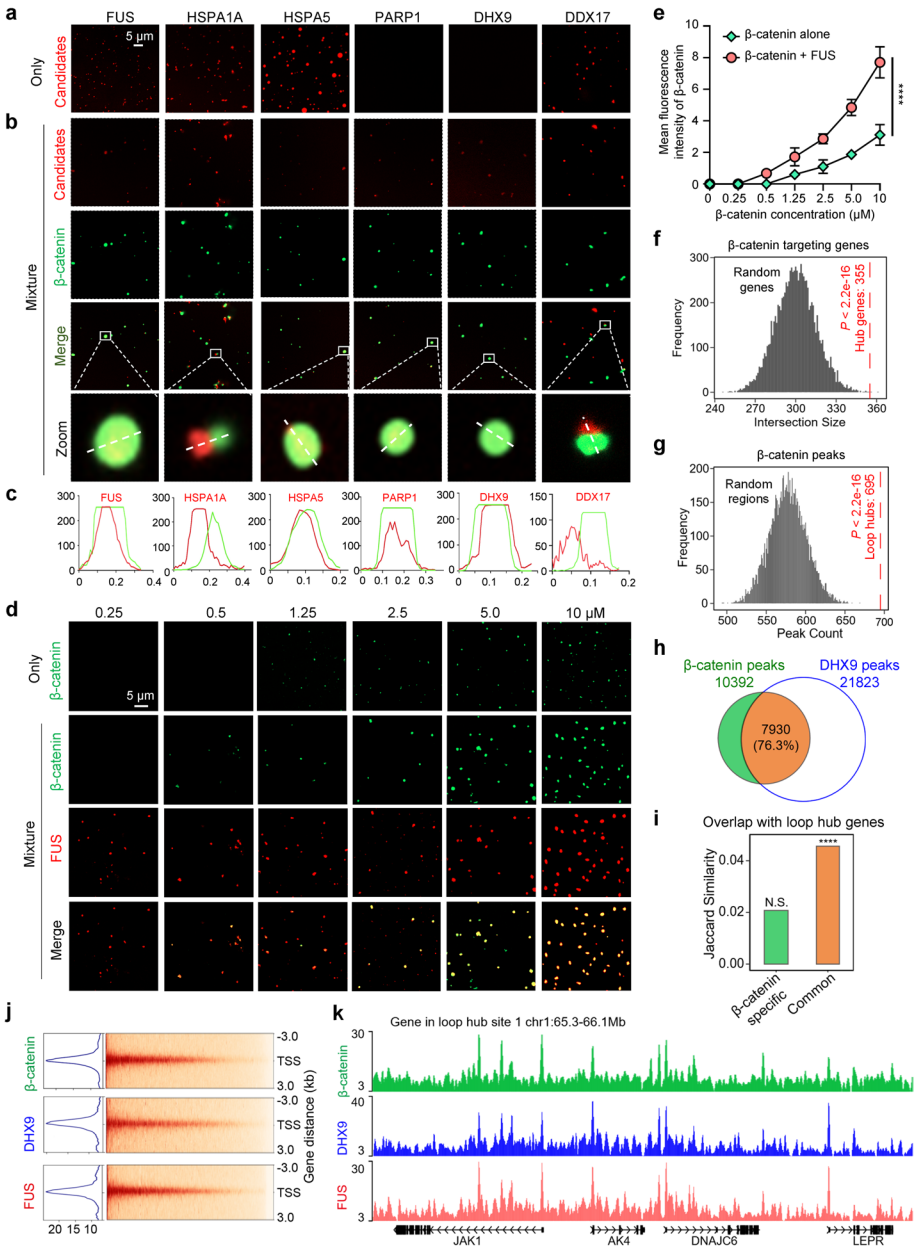

Fig. 6 (See legend on previous page.)

concentration of β-catenin increases, the fusion and coalescence of FUS and β-catenin became more pronounced (Fig. 6d). Moreover, both the number and size of the droplets formed by β-catenin together with FUS were greater than those formed by β-catenin alone at same concentration (Fig. 6d, e). These results support that FUS facilitates the formation of stronger β-catenin condensates. By contrast, mixing β-catenin with the client component PARP1 did not significantly impact β-catenin droplet formation (Additional file 1: Fig. S6d, e). In addition, we previously reported that scaffold proteins possess higher degree of protein–protein interaction (PPI) than non-phase-separated proteins [29], which was calculated based on the PPIs from the HIPPIE database [31]. In the PPI network containing all the components, the PPI degrees of FUS, β-catenin

and PARP1 decreased sequentially (Additional file 1: Fig. S6f, g), further indicating that phase separation ability of FUS is stronger than that of the latter two.

Taken together, these results demonstrate that among the identified components, FUS functions as a scaffold, whereas PARP1 functions as a client for β-catenin condensates.

Co-localization of component proteins with β-catenin at loop hubs

To elucidate the relationship between β-catenin and loop hubs, we performed β-catenin ChIP-seq to map its genomic binding sites. Firstly, we evaluated the association between β-catenin targeting genes and loop hub genes. As a control, we randomly selected genes equal in number to the loop hub genes. Our analysis revealed that β-catenin targeting genes exhibited a higher overlap with the loop hub genes than did the randomly selected genes (Fig. 6f). Secondly, we evaluated the correlation between β-catenin genomic binding and loop hub regions. As a control, we randomly selected genomic regions matching in length to the loop hub regions. Our results showed that β-catenin peaks were more enriched in loop hub regions than in randomly selected regions (Fig. 6g). These results demonstrate that β-catenin genomic binding is closely associated with loop hubs.

To further validate the cooperative effects of these components with β-catenin, we performed ChIP-seq for DHX9 and FUS and compared their binding profiles with that of β-catenin (Additional file 5: Table S4). Our results showed a substantial overlap between β-catenin peaks and those of DHX9 and FUS (Fig. 6h, j and Additional file 1: Fig. S6h), indicating that these proteins may function in concert. Moreover, by dividing β-catenin peaks into those overlapping with DHX9 peaks and those that do not, we observed that loop hub genes were predominantly occupied by the overlapping peaks rather than by β-catenin-specific peaks (Fig. 6i). These findings demonstrate that β-catenin and its component proteins co-localize within loop hubs, where they likely synergize to regulate gene expression (Fig. 6j).

Loss of key component proteins alters the transcriptional landscape within β-catenin condensates

To dissect the roles of the scaffold and client components in β-catenin condensates, we employed a CRISPR/Cas9-based gene editing tool to knock out (KO) the genes encoding FUS or PARP1 (Additional file 1: Fig. S7a-c). Knockout efficacy was rigorously validated by western blotting, DNA sequencing, and TA clone assays (Additional file 1: Fig. S7d-h), confirming that CRISPR/Cas9-induced insertion-based frameshift mutations resulted in effective silencing of FUS and PARP1 expression. Deletion of these components did not induce significant changes in the expression of other components (Additional file 1: Fig. S7i, j). Notably, deletion of FUS significantly attenuated β-catenin condensates, whereas PARP1 KO had no significant effect on condensate assembly (Fig. 7a, b). These observations further support that FUS functions as a scaffold to maintain the structural integrity of β-catenin condensates. Functionally, deletion of either FUS or PARP1 significantly inhibited CRC cell growth (Fig. 7c), suggesting that, although both perturbations converge on tumor suppression, they do so via distinct mechanisms. Moreover, attenuated β-catenin condensates caused by FUS KO resulted in reduction in loop strength within loop hubs (Fig. 7d), which was consistent with the role of phase separation in the

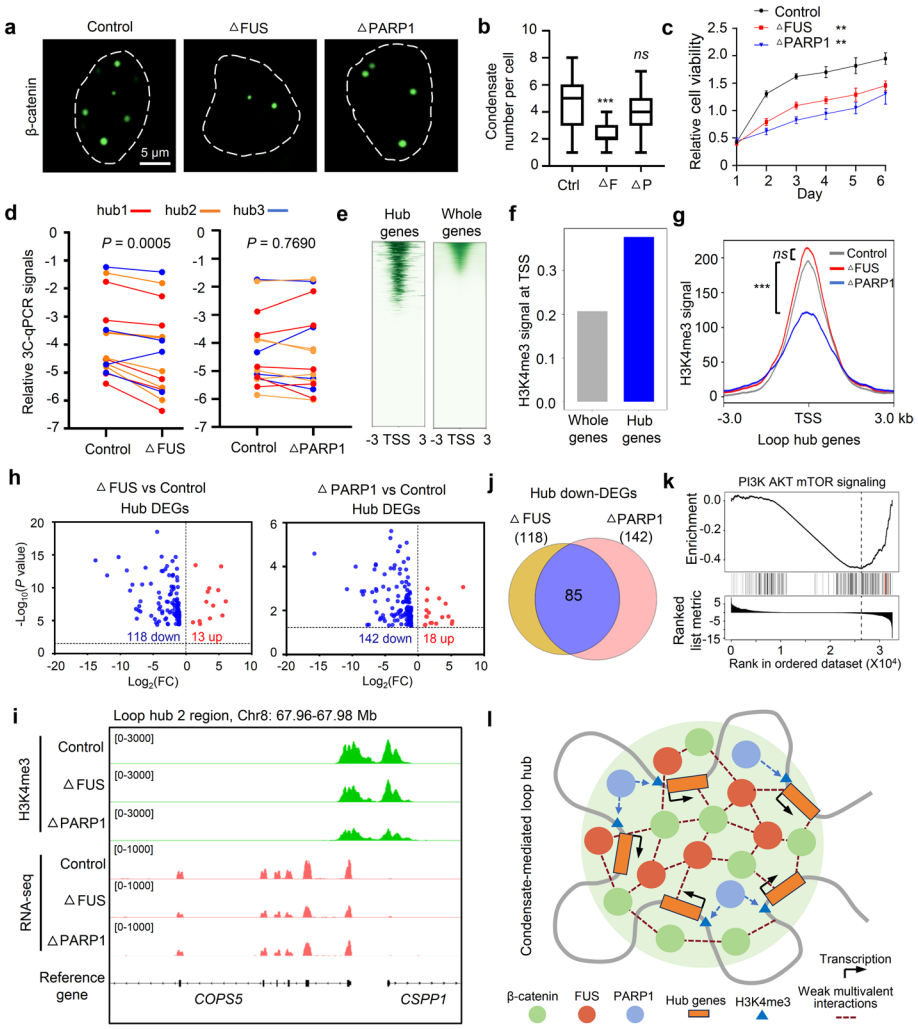

Fig. 7 Loss of the components attenuates the function of β-catenin condensates. **a** Representative image showing the alteration of eGFP-β-catenin condensates in response to loss of FUS or PARP1. Scale bars: 5um. **b** Quantification of the numbers of eGFP-β-catenin condensates in response to FUS or PARP1 deletion in HCT116 cells. ***$P < 0.001$ compared to control. *ns* means no significant change compared to control. **c** Cell viability of HCT116 cells with deletion of FUS or PARP1 and control cells were determined by CCK8 assay. Values are mean ± SD from three independent experiments. **$P < 0.01$ compared to control. **d** 3C-qPCR showing decreased DNA-DNA interactions at loop hub 1–3 in response to FUS deletion. KO of PARP1 does not significantly influence loop strength in the loop hubs. Three independent experiments are performed for 3C-qPCR. **e** Heatmaps of H3K4me3 peaks sorted for the TSS regions of loop hub genes (left) and whole genome genes (right) by CUT&Tag. **f** Proportion of H3K4me3 signals at TSS regions of whole genome genes (left) and loop hub genes (right) by CUT&Tag. **g** Average CUT&Tag read density of H3K4m3e around the TSS region of loop hub genes in control HCT116 cells and the cells with FUS or PARP1 deletion. ***$P < 0.001$ compared to control. *ns* means no significant change compared to control. **h** Scatter plot showing gene expression fold change and *P* value of loop hub genes in response to FUS (left) or PARP1 (right) deletion. **i** H3K4me3 distribution profiles by CUT&Tag and representative gene expression by RNA-seq at the loop hub 2 in HCT116 control cells and the cells with FUS or PARP1 deletion. **j** Venn diagram showing most down-regulated DEGs in response to FUS or PARP1 deletion are overlapped. **k** Gene Set Enrichment Analysis (GSEA) showing enriched biological pathways among the 85 shared down-regulated DEGs within loop hubs after FUS or PARP1 deletion. The analysis highlights the PI3K/AKT/mTOR signaling pathway as significantly impacted by loss of these components, underscoring the shared and distinct roles of FUS and PARP1 in β-catenin signaling and transcriptional regulation. Red vertical lines indicate the DEGs (MET, LAMC2, and LAMA2) that are consistently down-regulated upon deletion of FUS and PARP1. **l** Picture showing scaffold and client components function differentially to assemble condensates and active loop hubs

assembly of these regulatory structures [32]. In contrast, PARP1 depletion did not significantly influence the structural properties of loop hubs (Fig. 7d). We noted that higher H3K4me3 signals were enriched at the transcription start sites (TSSs) of genes within loop hubs than across the genome (Fig. 7e, f and Additional file 6: Table S5), further supporting that the internal environment of loop hubs was transcriptionally active. We then investigated the impact of these KOs on this epigenetic modification. Strikingly, loss of PARP1, but not FUS, led to a significant reduction in H3K4me3 levels at the TSS of loop hub genes (Fig. 7g). This finding indicates that PARP1 is critical for maintaining the active transcriptional environment within loop hubs. Consequently, KO of either FUS or PARP1 resulted in significant downregulation of numerous loop hub genes (Fig. 7h-j and Additional file 7: Table S6), which were functionally enriched in cancer-related signaling pathways, such as PI3K/AKT and mTOR signaling (Fig. 7k).

In summary, our results demonstrate a compelling uncoupling of mechanisms: the scaffold protein FUS is indispensable for the physical formation of the condensate-based loop hubs, while the client protein PARP1 is critical for establishing the active epigenetic landscape within them. Both are essential for the full transcriptional output of this phase separation-mediated gene regulatory network (Fig. 7l). These new insights provide a detailed and nuanced understanding of how biomolecular condensates coordinate gene expression in cancer.

Discussion

Cancer is largely driven by the activation of oncogenes or the inactivation of tumor suppressor genes. However, it is unlikely that tumorigenesis results from the overexpression or silencing of a single cancer-related gene. Instead, cancer likely arises from the synergistic dysregulation of multiple genes. Loop hubs, assembled through the phase separation of cancer-related factors, offer an elegant mechanism to interconnect multiple genes and coordinate large-scale transcriptional regulation. The hub structures are often assembled at genomic regions enriched by cell identity genes [33, 34], indicating these structures are crucial for cell fate determination. β-catenin is a key oncogenic factor in CRC that regulates multiple downstream targets. β-catenin does not have DNA-binding activity, and the conventional model for β-catenin genomic binding depends on TCF/LEF factors. However, neither a high percentage of the overlapped genes between the DEGs after β-catenin deletion and the loop hub genes (Fig. 2c) nor the presence of TCF/LEF in β-catenin condensates (Fig. 5e) was observed, indicating that the phase-separated model of β-catenin differs from the TCF/LEF-dependent genomic binding model. It has previously been shown that β-catenin can be incorporated into condensates through dynamic interactions, which occurs in the absence of TCF/LEF factors [20]. Perturbation of either β-catenin condensates or loop hubs suppresses the expression of loop hub genes and CRC cell growth, supporting the importance of both condensates and the genomic structures in maintaining the cancer phenotype.

Although β-catenin alone possesses some phase separation capacity, this ability is limited and insufficient to support the entire oncogenic regulatory network. For instance, the loop hubs mediated by β-catenin are large-scale genomic structures, usually at megabase (Mb) scale, and widely distributed across the cancer genome. To support these structures, more and larger β-catenin condensates are needed, which cannot be

generated without the support of scaffold proteins. Under this situation, FUS that exhibits robust phase separation capability [35, 36] is critical for the formation of functionally competent β-catenin condensates. Therefore, strictly speaking, it is more appropriate to describe FUS as the scaffold protein for oncogenic β-catenin condensates rather than physiological β-catenin condensates. Another concern is that, despite most β-catenin binding peaks being co-occupied by FUS, FUS peaks outnumber those of β-catenin. This observation suggests that, in addition to serving as a scaffold for the assembly of the oncogenic β-catenin condensates, FUS may have other functions in CRC that are independent of β-catenin. As arginine methylation is well known to modulate FUS phase separation [37, 38], this post-translational modification may support the independent functions of FUS, which warrants further investigation.

Both scaffold and client components contribute to the functional properties of condensates, albeit through distinct mechanisms. While scaffold proteins are primarily responsible for building an environment for the entire regulatory network, client proteins determine the internal characteristics of this environment [39]. In this context, PARP1 and DHX9 likely function as client proteins, as they are not capable of independent phase separation but are readily recruited into β-catenin condensates. Furthermore, our findings reveal that genes within loop hubs are largely co-occupied by β-catenin and H3K4me3-marked loops, indicating that transcriptional activation rather than repression is predominant within these condensates. A key question remains: which components are essential for maintaining the active chromatin environment within phase-separated condensates? Is it the scaffold proteins that are intrinsically resistant to repressive heterochromatin, or the client proteins that directly modulate epigenetic modifications? Our data suggest that client components, particularly PARP1, are critical for sustaining an active environment. PARP1 has dual roles in establishing and maintaining H3K4me3 modification. On the one hand, PARP1 can recruit chromatin remodeling complexes to loosen the chromatin structure in the promoter region of TET1, facilitate the access of the SET1/MLL family protein complex to H3K4, promote the establishment of H3K4me3 marks [40]. On the other hand, PARP1 maintains the level of H3K4me3 by PARylating, inhibiting, and excluding the histone demethylase KDM5B [40]. Therefore, the enzymatic activity of PARP1 is required for both recruiting the enzyme complexes responsible for adding H3K4me3 marks and preventing the demethylation of H3K4me3.

Identifying the components and clarifying the role and functional links among different components are crucial for us to explore the biological functions of phase separation. We have verified that phase separation directly regulates genome organization for cell fate transitions [12]. How pathologic phase separation regulates aberrant genome structures in tumorigenesis remains to be clarified. Future in vivo studies will be carried out to validate the influence of this mechanism in tumor progression. Employing the patient-derived xenografts (PDXs) carrying the loop hub structures or not, or the cell-derived xenografts (CDXs) whose loop hubs were perturbed in vitro, the tumorigenicity between different groups would be evaluated through tumor incidence and burdens, as well as vital status of mice. Addressing these points will deepen our understanding of the interplay among phase separation, epigenetic regulation, and genome organization in orchestrating large-scale gene expression in cancer.

Conclusions

In conclusion, our study demonstrates that β-catenin-associated active loop hubs are crucial for CRC growth. We show that phase separation of β-catenin plays a key role in forming these loop hubs. Additionally, our work identifies the component proteins of β-catenin condensates, highlighting FUS as a representative scaffold protein and PARP1 as a representative client protein. FUS is essential for facilitating condensate assembly, whereas PARP1 is crucial for maintaining an active transcriptional environment within the condensates. Together, these scaffold and client components synergistically support the oncogenic functions of β-catenin condensates in CRC.

Methods

Cell culture

HCT116 (Procell, #CL-0096), SW480 (Procell, #CL-0223) and SW620 (Procell, #CL0025) CRC cell lines are purchased from Procell Life Science & Technology Co., Ltd. (Wuhan, China). NCM460 were generously provided by Dr Huabin Gao at the First Affiliated Hospital, Sun Yat-Sen University [41]. These cells are cultured in DMEM medium with high glucose (ZETA, #BM0003), supplemented with 10% fetal bovine serum (FBS) (Cas9X, #FBP-C520) and 1% Penicillin–Streptomycin (Gibco, #15,140,122). For subculture, the medium was removed and the cell surface was washed twice with PBS. The adherent cells were then digested by trypsin, neutralized by FBS, and collected by centrifugation at 1250 rpm for 3 min. The cells were resuspended with fresh medium and planted in the 100 mm Petri dish culture in the 37 °C, 5% CO2 incubator. Before the experiments were performed, the identity of cell lines was verified via short tandem repeat analysis, and the cells were confirmed to be mycoplasma-negative.

FUS or PARP1 deletion HCT116

To knock out the targeting genes, HCT116 cells were planted into 6-well plates, and the PCA25-Cas9-sgRNA-eGFP vector (Addgene, #62,988) were transfected using Lipofectamine 3000 (Invitrogen, #L3000150). The resultant cells were incubated at 37 °C for 2–4 days, and the single cells with green fluorescence were sorted by flow cytometry. The sorted cells were expanded over several days to reach enough. Protein was extracted and KO efficacy was validated by western blots. For the cell clones showing loss of target protein by western blots, genomic DNA was extracted. The forward and reverse primers were designed 250 bp upstream or downstream of the sgRNA targeting site for TA cloning. PCR was performed using Taq polymerase (GenStar, #A002-10). An "A" base was added at the 3' end of the products, and these fragments were cloned into a pESI-T vector using Hieff Clone® Zero TOPO-TA Cloning Kit (YEASEN, #10907ES08), followed by transform into DH5α cells. After incubating at room temperature for 5 min, LB medium was added and cultured at 37 °C with shaking, followed by plating the cultures to screen single colonies. Transfer single colonies into a PCR mix for amplification with the original primers and send the products to Tsingke Biotech for sequencing. Successful KO was confirmed if sequencing reveals two frameshift mutations different from the original sequence, and the successfully KO cells can be used for further experiments.

HCT116 cells carrying dCas9-KRAB-MeCP2

HCT116 cells were planted into the 6-well plate and allow them to grow until covering 60–70% confluency. Then dCas9-KRAB-MeCP2 and sgRNA vectors were co-transfected into the cells using the jetPRIME transfection reagent (Polyplus, # 101000046). In brief, the transfection mixture was prepared according to the reagent instructions and let it stand for 10 min. In this time, the cell culture medium was removed and replaced with serum-free DMEM. The transfection mixture was slowly and evenly dropwise added into the wells. After 5 h, the medium was replaced with serum-containing medium. The cells were incubated at 37 °C for 2–3 days before collecting for bisulfite sequencing.

Human samples

Paired paraffin-embedded adjacent normal and CRC tissue were collected for β-catenin condensate analysis. Written informed consent was obtained from all patients involved in this study at the Sixth Affiliated Hospital of Sun Yat-sen University before sample collection. All experimental procedures involving human samples in this study have been approved by the ethical committee of the Sixth Affiliated Hospital of Sun Yat-sen University (2023ZSLYEC-002). All procedures were performed in compliance with relevant laws and institutional guidelines.

HiChIP

HiChIP was performed with some modifications. Ten million cells were cross-linked for 10 min at room temperature with 1% formaldehyde in growth media and quenched in 0.125 M glycine. Cross-linked cell pellets were resuspended in 500 ul of ice-cold HiC lysis buffer (10 mM Tris–HCl pH 8.0, 10 mM NaCl, and 0.2% IGEPAL CA-630) with protease inhibitor (Roche, #1,169,749,800), and incubated at 4 °C for 30 min. Nuclei were pelleted and washed once with 500ul of ice-cold HiC lysis buffer. After removing supernatant, nuclei were incubated in 100ul of 0.5% SDS at 62 °C for 10 min. SDS was quenched by adding 285ul water and 50ul 10% Triton X-100, and nuclei were incubated for 15 min at 37 °C. After addition of 50ul of 10 × NEB Buffer 2 and 375 U of MboI, chromatin was digested at 37° overnight. MboI enzyme was then inactivated by incubating at 62 °C for 20 min. To fill in the restriction fragment overhangs and mark the DNA ends with biotin, 52ul of fill-in master mix containing 37.5ul of 0.4 mM biotin-dATP, 1.5ul of 10 mM dCTP, 1.5ul of 10 mM dGTP, 1.5ul of 10 mM dTTP, and 10ul of 5 U/ul DNA Polymerase I, Large (Klenow) Fragment was added and incubated at 37 °C for 1 h with rotation. Proximity ligation was performed by incubating in a solution of 947ul of ligation master mix containing 150ul of 10X NEB T4 DNA ligase buffer, 125ul of 10% Triton X-100, 7.5ul of 20 mg/mL BSA (Sigma, #A7906), 10ul of 400 U/ul T4 DNA ligase and 655.5ul of water at room temperature for 4 h with rotation. After proximity ligation, nuclei were pelleted and resuspended in 1 ml of ChIP sonication buffer (50 mM HEPES–KOH pH 7.5, 140 mM NaCl, 1 mM EDTA pH 8.0, 1 mM EGTA pH 8.0, 1% Triton X-100, 0.1% sodium deoxycholate, and 0.1% SDS) with protease inhibitor. Nuclei were sonicated using a Covaris S220. 60ul of protein G magnetic beads were washed three times with sonication buffer, resuspended in 50ul of sonication buffer, and added to the sonicated chromatin and incubated for 1 h at 4 °C with rotation. Beads were then separated on a magnetic stand and the supernatant was mixed with 7.5 ug antibody,

and incubated overnight at 4 °C with rotation. 60ul of protein G magnetic beads were washed and resuspended in 100ul of sonication buffer. Samples were incubated with the beads for 2 h at 4 °C with rotation. Beads were then separated on a magnetic stand and washed three times with 1 ml of high salt sonication buffer (50 mM HEPES–KOH pH 7.5, 500 mM NaCl, 1 mM EDTA pH 8.0, 1 mM EGTA pH 8.0, 1% Triton X-100, 0.1% sodium deoxycholate, 0.1% SDS) followed by three times with 1 ml of LiCl wash buffer (20 mM Tris–HCl pH 8.0, 1 mM EDTA pH 8.0, 250 mM LiCl, 0.5% IGEPAL CA-630, 0.5% sodium deoxycholate, 0.1% SDS) and once with 1 ml of TE buffer (10 mM Tris–HCl pH 8.0, 1 mM EDTA pH 8.0, 50 mM NaCl). Beads were then resuspended in 200ul of elution buffer (50 mM Tris–HCl pH 8.0, 10 mM EDTA pH 8.0, 1% SDS) and incubated at 65 °C for 15 min to elute. To purify eluted DNA, RNA was degraded by incubation with 2.5ul of 33 mg/mL RNase A (Thermo, #EN0531) at 37 °C for 2 h. Protein was degraded by incubation of 10ul of 20 mg/mL proteinase K (Invitrogen, #25,530,049) at 55 °C for 45 min. Samples were then incubated at 65 °C for 5 h to reverse cross-links. Phenol: chloroform: isoamyl alcohol extraction was performed followed by an ethanol precipitation. The DNA was then resuspended in TE buffer. Tagmentation of ChIP DNA was performed using the Tn5 (Vazyme, #TD501). First, 5ul of streptavidin T1 magnetic beads (Invitrogen, #65,601) was washed with 1 ml of tween wash buffer (5 mM Tris–HCl pH 7.5, 0.5 mM EDTA pH 8.0, 1 M NaCl, 0.05% Tween-20) and resuspended in 10ul of 2 × biotin binding buffer (10 mM Tris–HCl pH 7.5, 1 mM EDTA pH 8.0, 2 M NaCl). 125 ng purified DNA was added in a total volume of 10ul of water to the beads and incubated at room temperature for 15 min with agitation every 5 min. After capture, beads were separated with a magnet and the supernatant was discarded. Beads were then washed twice with 500ul of tween wash buffer at 55 °C for 2 min. After washes, beads were resuspended in 1 × TTBL. Tn5 amount was adjusted linearly for different amounts of post-ChIP DNA, 125 ng of DNA was transposed with 4ul of Tn5. Samples were incubated at 55 °C with interval shaking for 10 min. Beads were then placed on a magnet, and supernatant was removed. 50 mM EDTA was added to samples and incubated with interval shaking at 50 °C for 30 min. Samples were washed in 10 mM Tris, pelleted and resuspended for PCR amplification (Vazyme, #TD202). Two biological replicates were performed for each cell line.

In situ 3C

3C was performed as previously described [42]. Cells were crosslinked with 1% formaldehyde for 10 min at room temperature. Cells were resuspended in 500ul of lysis buffer (10 mM Tris–HCl pH8.0, 10 mM NaCl, 0.2%Igepal CA630, protease inhibitors cocktail) and incubated for 15 min at 4 °C. Cells were washed twice in lysis buffer and incubated in 50ul of 0.5% SDS at 65 °C for 8 min. SDS was quenched by incubating in a solution of 25ul of 10% Triton-X and 145ul H_2O at 37 °C for 15 min. 25ul of 10 × NEBuffer2 and 20ul of MboI were added and the chromatin was digested at 37 °C overnight with rotation. To inactivate MboI, the sample was incubated at 65 °C for 20 min. Restriction fragments were biotinylated by supplementing the reaction with 1.5ul dNTP, 8ul of DNA polymerase I, large (Klenow) fragment, 40.5ul H2O and incubated at 37 °C for 4 h. The end-repaired chromatin was added into a solution of 663ul H_2O, 120ul NEB T4 ligase

buffer, 100ul 10% Triton-X 100, 12ul 10 mg/ml BSA, 5ul T4 DNA ligase. The ligation was performed for 4 h at room temperature with rotation. Crosslinks were reversed by adding 50ul of 20 mg/ml proteinase K, 120ul 10% SDS at 55 °C for 30 min, and another addition of 130ul 5 M NaCl at 68 °C overnight. The DNA was precipitated with ethanol and resuspended in Tris-buffer for about 100 ng/ul DNA. 100 ng DNA were amplified in PCR for 35 cycles. Primers used are listed in Additional file 8: Table S7.

ChIP-seq

1% formaldehyde in PBS was used to crosslink the cells for 10 min, followed by quenched with 125 mM glycine on ice. Cells were collected and flash frozen in liquid nitrogen, then stored at −80 °C for use. Frozen crosslinked cells were thawed on ice and then resuspended in lysis buffer I (50 mM HEPES–KOH, pH 7.5, 140 mM NaCl, 1 mM EDTA, 10% glycerol, 0.5% NP-40, 0.25% Triton X-100, protease inhibitors). After rotated for 10 min at 4 °C, the cells were collected, and resuspended in lysis buffer II (10 mM Tris–HCl, pH 8.0, 200 mM NaCl, 1 mM EDTA, 0.5 mM EGTA, protease inhibitors). After rotated for 10 min at 4 °C, the cells were collected, and resuspended in sonication buffer (20 mM Tris–HCl pH 8.0, 150 mM NaCl, 2 mM EDTA pH 8.0, 0.1% SDS, and 1% Triton X-100, protease inhibitors) for sonication. Sonicated lysates were cleared once by centrifugation at 16,000 g for 10 min at 4 °C. Input material was reserved. The remainder was incubated with magnetic beads bound with antibody to enrich for DNA fragments overnight at 4 °C. Beads were washed with wash buffer (50 mM HEPES–KOH pH 7.5, 500 mM LiCl, 1 mM EDTA pH 8.0, 0.7% Na-Deoxycholate, 1% NP-40) and TE buffer (10 mM Tris–HCl pH 8.0, 1 mM EDTA, 50 mM NaCl) in order. Beads were removed by incubation at 65 °C for 30 min in elution buffer (50 mM Tris–HCl pH 8.0, 10 mM EDTA, 1% SDS). Cross-links were reversed overnight at 65 °C. To purify eluted DNA, 200 ml TE was added and then RNA was degraded by incubation in 8ul 10 mg/ml RNase A at 37 °C for 2 h. Protein was degraded by addition of 4ul 20 mg/ml proteinase K and incubation at 55 °C for 2 h. Phenol: chloroform: isoamyl alcohol extraction was performed followed by an ethanol precipitation. The DNA was then resuspended in 70ul 10 mM Tris–HCl (pH 8.0). DNA concentration was measured by Qubit, and proceed to high-throughput sequencing.

CUT&Tag

Using the Hyperactive Universal CUT&Tag Assay Kit for Illumina Pro (TD904-01) [43], approximately 100,000 cells were utilized to generate in situ protein-DNA binding profiles. Reagents were proportionally prepared based on the sample size. Specifically, one Sigma-Aldrich protease inhibitor cocktail tablet (Cat# 5,056,489,001) was dissolved in 1 ml of ddH_2O and stored at −20 °C. Binding Buffer was prepared by diluting 30 µl of 10 × Binding Buffer in 270 µl of ddH_2O, while Wash Buffer was prepared by mixing 150 µl of 10 × Wash Buffer with 30 µl of 50 × protease inhibitor and 1,320 µl of ddH_2O. Antibody Buffer was created by combining 50 µl of Antibody Buffer (-) with 0.5 µl of 5% Digitonin, which was pre-chilled on ice. Additionally, Dig-wash Buffer was prepared by mixing 792 µl of Wash Buffer with 8 µl of 5% Digitonin, and Dig-300 Buffer was prepared by combining 100 µl of 10 × Dig-300 Buffer with 2 µl of 5% Digitonin, 20 µl of 50 × protease inhibitor, and 878 µl of ddH_2O. Cells were collected, counted, and transferred to

1.5 ml microcentrifuge tubes, centrifuged at 600 × g for 5 min at room temperature, and the supernatant was discarded. The cells were resuspended in 100 μl of pre-chilled NE Buffer, incubated on ice for 10 min, and then centrifuged again at 600 × g for 5 min. The supernatant was discarded, and nuclei were resuspended in 100 μl of Wash Buffer. Activated ConA Beads Pro (10 μl) were added to 100 μl of Binding Buffer in an 8-tube strip, mixed thoroughly, placed on a magnetic rack until the solution cleared, and the supernatant was discarded. The process was repeated, and the beads were finally resuspended in 10 μl of Binding Buffer. The nuclei were transferred to the tube containing the activated beads, mixed by inversion, and incubated at room temperature for 10 min, with gentle mixing every few minutes. The bead-nuclei complexes were resuspended in 50 μl of pre-chilled Antibody Buffer, the primary antibody was added, and the mixture was incubated overnight at 4 °C with gentle agitation. The following day, secondary antibody diluted in Dig-wash Buffer was added, and the samples were incubated at room temperature with rotation for 30–60 min. After brief centrifugation, the supernatant was discarded, and the complexes were washed three times with Dig-wash Buffer. Then, 100 μl of pA/G-Tnp Pro transposase mix was added to each sample, and the mixtures were incubated at room temperature for 1 h with rotation. Following brief centrifugation and supernatant removal, the samples were washed three times with Dig-300 Buffer. For DNA elution and purification, 50 μl of TTBL Buffer was added, and the samples were incubated at 37 °C for 60 min. Subsequently, 2 μl of 10% SDS and an appropriate amount of DNA Spike-in were added, mixed thoroughly, and incubated at 55 °C for 10 min. The supernatant was collected using a magnetic rack and transferred to a new tube containing activated DNA Extract Beads Pro. After a 20 min incubation at room temperature, the beads were washed twice, air-dried, and the DNA was eluted in 15 μl of ddH_2O. The resulting samples were either stored at −30 to −15 °C or immediately used for subsequent library preparation and PCR amplification according to the kit's instructions.

RNA-seq

Using RNA-easy for intracellular RNA extraction, approximately 5 million cells were collected for each replicate, and RNA was extracted using the RNA-easy Isolation Reagent according to the manufacturer's instructions. For library construction and sequencing, the samples were outsourced to the professional company Novogene. The samples were prepared as described and then shipped to Novogene, where they performed library construction and sequencing according to their standard protocols, ensuring high-quality results suitable for downstream applications.

Bisulfite sequencing

DNA methylation changes at loop hubs in response to dCas9-KRAB-MeCP2 were evaluated by bisulfite sequencing. In brief, DNA was extracted from HCT116 cells in which the selected loop hubs were targeted by dCas9-KRAB-MeCP2 via guide RNAs (TIANGEN, #DP304-02), followed by bisulfite treatment for 60 min (TIANGEN, #DP215-02). PCR amplification was performed using ZymoTaq™ premix (Zymo Research, #E2003-1). Direct Sanger sequencing of the PCR products was used to evaluate methylation levels at multiple CpG sites. The proportion of methylation was calculated as the peak ratio of

cytosine to the sum of cytosine and thymine at each site. Primers used are listed in Additional file 8: Table S7.

dCas9-APEX2 MS

PB-TRE-dCas9-APEX2 and sgRNA vectors were co-transfected into the cells using the jetPRIME transfection reagent (Polyplus, # 101,000,046). 24 h after transfection, the cells were incubated in 2 ml of 500 μM biotin-phenol (BP) and for 30 min at 37 °C (preparation of 1000X stock solution by dissolving 0.37 g BP in 2 ml DMSO, then add 3 μl of the 1000X BP stock to 3 ml of complete medium). Next, the appropriate amount of hydrogen peroxide (H_2O_2) was added directly to the BP solution, giving a brief mix to achieve a final concentration of 1 mM, and incubated the cells at room temperature for 1 min. Quickly aspirated the labeling solution and washed the cells three times with 2 ml of quencher solution (prepared by dissolving 198 mg of sodium ascorbate (Aladdin, #S105024) in 1 ml of water, adding 125 mg of Trolox to 1 ml of DMSO, and mixing 500 μl each with 49 ml DPBS). Use 2 ml of fresh quencher solution to scrape the cells off the bottom of the well. Pelleted the cells by centrifugation for 10 min at 3,000 g at 4 °C, then removed the supernatant. Lysed the cell pellets by pipetting in 100–200 μl of RIPA lysis buffer supplemented with 1 × protease inhibitor cocktail, 1 mM PMSF, and quenchers (10 mM sodium azide, 10 mM sodium ascorbate, and 5 mM Trolox). Leaving the cells on ice for 5–10 min, then clarify the lysates by centrifuging at 15,000 g for 10 min at 4 °C. For each sample, take 100 μl aliquots of streptavidin magnetic beads (Invitrogen, #65,601), washing each aliquot twice with 1 ml of RIPA lysis buffer. Incubate each lysate sample with 100 μl of streptavidin magnetic beads for 1 h at room temperature on a rotator, adding 500 μl of RIPA buffer to facilitate mixing. Using a magnetic rack to pellet the beads and wash each bead sample with a series of buffers (1 ml per wash) to remove nonspecific binders: twice with RIPA lysis buffer, once with 1 M KCl, once with 0.1 M Na2CO3, once with 2 M urea in 10 mM Tris–HCl, pH 8.0, and twice again with RIPA lysis buffer. The biotinylated proteins were eluted from the beads by boiling each sample at 100 °C in 100 μl of elution buffer consisting of 5 × protein loading buffer supplemented with 2 mM biotin and 20 mM DTT for 10 min. Briefly vortex the beads, cooled the samples on ice, and spined down briefly to eliminate condensation. Using a magnetic rack to pellet the beads and collect the eluate, placing the eluates on ice. Samples were then fractionated on a 10% NuPAGETM 4–12% Bis–Tris Gel (Thermo Scientific, #NP0009) and stained with GelCodeTM Blue Safe Protein Stain buffer (Thermo Scientific, #24,594). The products from a single purification were subjected to whole lane LC–MS/MS sequencing and data analysis. sgRNAs used are listed in Additional file 8: Table S7.

DNA extraction and PCR

Genomic DNA is extracted from the cells using the TIANamp Genomic DNA Kit (TIANGEN, #DP304). In brief, the cell pellets were resuspended in a mixture solution including 200ul Buffer GA, 20ul Proteinase K solution and 200ul Buffer GB, and incubated at 70 °C for 10 min. Then 200ul absolute ethanol was added and the genomic DNA was cleaned by mix by CB3 spin column. The purified genomic DNA was collected in 100 μL TE Elution Buffer. To amplify the targeting genome regions, PCR was performed

using the 2 × Phanta Flash Master Mix (Dye Plus) (Vazyme, #P520-01). Primers used are listed in Additional file 8: Table S7.

RNA isolation and qRT-PCR

Total RNA was extracted from cell pellets using SteadyPure Universal RNA Extraction Kit (AG, #AG21017). Complementary DNA (cDNA) synthesis and removal of genomic DNA were both carried out using the Evo M-MLV RT Kit(AG, #AG11705). Real time qPCR was performed using SYBR Green Premix Pro Taq HS qPCR Kit (AG, #AG11701) on LightCycler 480 II system. The exhibited data represents the fold change (FC) of experimental group vs. control group. In brief, Ct was calculated as Ct = Ct (test gene)—Ct (Ref. gene). Ct was calculated as Ct = Ct (experimental group)—Ct (control group). The FC of a test gene in experimental group vs. control group was calculated as FC = 2^(-Ct). Each gene tested in triplicates in every independent experiment, and all experiments were triplicated. Primers used are listed in Table S7.

Protein extraction and western blots

Cells were lysed in Cytobuster (Millipore, #134,044) at room temperature for 10 min. Lysate was separated on 10% Bis–Tris gel, and then wet transferred to a 0.45 um PVDF membrane (Bio-rad, #1,620,177) in ice-cold transfer buffer for 6 h. After blocked with 5% non-fat milk in TBS for 1 h at room temperature, the membrane was incubated with the primary antibody overnight at 4 °C. After washed three times with TBST, the membrane was incubated with 1:2000 secondary antibodies for 1 h at room temperature. After washed three times with TBST. The membrane was developed with ECL substrate and imaged using a CCD camera or exposed using film or with high sensitivity ECL (Bio-rad, #170–5061).

Immunofluorescence

Cells were plated in glass bottom culture dish, washed twice with cold PBS. The cells were fixed using 4% paraformaldehyde for 15 min at room temperature. Then paraformaldehyde was removed and the cells were permeabilized by 0.5% Triton X-100 for 5 min. Cells were blocked with 600 μl 5% BSA for 1 h at room temperature. After aspirating blocking buffer, primary antibody was added at a certain concentration in antibody buffer at 4 °C overnight. Cells were washed with PBS three times followed by incubation with labeled secondary antibody at a certain concentration of 1:200 in antibody buffer for 1 h at room temperature without light exposure. After two washes of PBS, cells were stained with 1 μg/ml DAPI (MCE, #HY-D0814) in PBS for 10 min at room temperature without light exposure. Finally, images were acquired at Zeiss Confocal microscope LSM 800.

For the paired paraffin-embedded slides of adjacent normal and CRC tissues, the slides were stained as previously described [44]. Primary antibody was diluted in 1:1000 for 12 h at 4 °C in a humidified chamber. Secondary antibody was diluted in 1:400. After secondary antibody incubation for 1 h, slides were washed three times and then stained with 1 μg/ml DAPI in PBS for 10 min at room temperature without light exposure. Finally, images were acquired at Zeiss Confocal microscope LSM 800. Images were post-processed using Fiji Is Just ImageJ (FIJI) 2.9.0.

SunTag

SunTag system was utilized to capture the amplified fluorescence at the loop bub sites. This system comprised of three plasmids: pSpdCas9(BB)−2A-Peptide epitopes plasmid and sgRNA plasmid are responsible for targeting the desired sites. pCMVp-scFV-BFP plasmid carrying a BFP fusion antibody can specifically bind with peptide epitopes for fluorescent signal amplification. In addition, this assay needs another plasmid carrying eGFP-β-catenin to locate nuclear condensate position. For the assay, HCT116 cells were planted into a 6-well plate and grow until they reach 60–70% confluency. The four plasmids were co-transfected using the jetPRIME transfection reagent (Polyplus, #101,000,046). Prepare the transfection mix according to the reagent instructions and let it sit for 10 min. Replace the cell culture medium with serum-free DMEM, then slowly and evenly add the transfection mix to the wells. After 5 h, switch to serum-containing medium. The cells were then incubated at 37 °C for 48 h and capture images using a confocal microscope. sgRNAs used are listed in Additional file 8: Table S7.

In vitro droplet formation

cDNA encoding the genes of β-catenin and the component proteins were cloned into pET28a expression vector. The base vector was engineered to include a 5′ 6xHIS followed by either GFP or mCherry and a 6 amino acid linker sequence "GGATCC." Vectors expressing GFP or mCherry alone contain the linker sequence followed by a STOP codon. The interest sequence was cloned into the vector at the position between the linker sequence and the STOP codon. All expression constructs were sequenced to ensure sequence identity. For protein expression, plasmids were transformed into BL21 E. coli (Gensand, #SEC19) and grown as follows. A fresh bacterial colony was inoculated into LB media containing kanamycin and grown overnight at 37 °C. Then the cells were diluted 1:30 in 300 ml LB with freshly added kanamycin and grown 2 h at 37 °C to make sure OD600 up to 0.6–0.8. Then temperature was decreased to 16 °C and IPTG (Solarbio, #I1020-5) was added to 0.3 mM and growth continued overnight. After centrifugation, cell pellets were resuspended in 15 ml of nondenaturing lysis buffer (Beyotime, #P2226-2) containing protease inhibitors (Sigma, #11,697,498,001) and sonicated (30 cycles of 30 s on, 15 s off). The lysates were cleared by centrifugation at 3,000 g for 30 min and added to 1 ml of BeyoGold™ His-tag Purification Resin (Beyotime, #P2226-1) that had been pre-equilibrated with 5 volumes of the same buffer. Tubes containing this agarose slurry were rotated for 1.5 h. The slurry was poured into a column, washed with 10 volumes of the washing buffer and eluted 6 X with elution buffer containing 250 mM imidazole. Each fraction was run on a 12% gel and proteins of the correct size were dialyzed by dialysis buffer (50 mM Tris pH 7.5, 125 mM NaCl, 1 mM DTT and 10% Glycerol. The Recombinant GFP or mCherry fusion proteins were concentrated in centrifugal filters (Millipore, #UFC903096) for use. The proteins with an appropriate concentration mixed with 10% PEG-8000 (Sigma, #89,510-250G-F), and solve in 125 mM NaCl (Sigma, #S5150-1L). The protein solution was immediately loaded onto a homemade chamber comprising a glass slide, and imaged with a fluorescence microscopy (Nikon Eclipse Ts2R-FL).

FRAP

HCT116 cells stably expressing β-catenin-GFP were cultured in gelatin-coated glass bottom dish for 24 h. Fluorescence images of GFP were acquired on a Nikon A1 + confocal microscope using a 100 × oil-immersion objective lens (HP Apo TIRF 100xH, 1.49 NA, Nikon). The fluorescence intensity of bleached cell at each time point was normalized by fluorescence intensity at background region and fluorescence intensity of adjacent unbleached cell. The images were analyzed using NIS-Elements software. The inner fluidity of in vitro droplets was also evaluated by FRAP.

Colony formation assay

Three thousand of HCT116 cells stably carrying dCas9-KRAB-MeCP2 and sgRNAs targeting loop hubs or control sgRNAs were planted on six-well plates with puromycin. After culturing for 10–14 days, the cells were fixed with 70% ethanol and stained with crystal violet solution. All experiments were conducted three times in triplicates.

CCK8 cell proliferation

Cell proliferation was assessed by cell viability using the Cell Counting Kit-8 (CCK8) (MCE, #244,902). Approximately 1×10^4 cells were planted in each well of a 96-well plate. Cell viability was measured for every 24 h until 7 days by the absorbance at 450 nm using a microplate reader. The experiment was conducted in three independent triplicates and results were shown as the means ± sd.

Quantification and statistical analysis

Quality control of sequencing reads

All Illumina sequencing reads used in this study underwent initial quality control using fastp (version 0.23.4) [45]. The quality control process involved trimming low-quality bases from both the 5' and 3' ends of the reads using sliding windows. Specifically, a sliding window was moved from the 5' end to the 3' end of each read, discarding bases within the window if the mean quality score fell below a specified threshold, and stopping once the mean quality score met or exceeded the threshold. Similarly, another sliding window was moved from the 3' end to the 5' end of each read, following the same criteria. The size of the sliding windows used in both trimming processes was set to 4 bases, as specified by the -W 4 parameter. This quality control step ensured that the sequencing reads retained high-quality bases for downstream analysis, thereby improving the reliability of the subsequent bioinformatics analyses.

ChIP-seq and CUT&Tag data analysis

We aligned the clean ChIP-seq or CUT&Tag data to the hg19 reference genome using 'bowtie2' (v2.5.1) with default parameters [46]. Post-alignment, we removed multiple aligned reads, low-quality reads, and PCR duplicates using 'samtools' (v1.16.1) [47]. The BAM files were then sorted and indexed using 'samtools'. Peaks were called using 'MACS2' (v2.2.7.1) with a false discovery rate (FDR) threshold of 0.01 to identify

significant binding sites [48]. Peaks were considered significant if they had an FDR below 0.01. To generate coverage files in BigWig format, we used 'deepTools' (v3.5.3) 'bamCoverage' with a bin size of 10 bases, normalizing using reads per kilobase per million mapped reads (RPKM). Replicates were incorporated into the analysis by merging BAM files from biological replicates using 'samtools merge'. Peak calling was performed on the merged files to ensure robustness and reproducibility of the detected peaks. The generated ChIP-Seq or CUT&Tag peaks were used for various bioinformatic analyses and data presentations. Overlap analysis of peaks from different conditions or samples was performed using 'bedtools intersect' (v2.31.1) [49]. Heatmaps and profile plots were created using 'deepTools', 'computeMatrix' and 'plotHeatmap' functions to visualize the distribution of ChIP-Seq or CUT&Tag signals around peaks or gene bodies.

RNA-Seq data analysis

The clean reads were mapped to the hg19 reference genome using STAR (v2.7.11a) with ENCODE option bundles. Uniquely mapped reads were counted using HTSeq-count (v2.0.3) [50]. The read counts were normalized using the trimmed mean of M values (TMM) method and transformed to reads per kilobase per million reads (RPKM) using edgeR (v3.40.0) [51]. An expression cutoff of RPKM > = 1 in at least one sample group was applied to remove low-abundance genes. Differentially expressed genes were identified using edgeR, with genes considered differentially expressed when the overall false discovery rate (FDR) was < 0.01 and the fold change was above 2.0.

APEX2 proximity labeling data analysis

Whole lane LC–MS/MS sequencing and peptide identification were performed at Shenzhen Wininnovate Bio Technology Company Limited, China. The detailed information for data analyses was referred to previously published works [52, 53]. Selection criteria for high confidence components within the condensates are as follows. First, for each loop hub, if the candidate is present at both pools of sgRNA1 and sgRNA2, but absent at control pool, the candidate is considered as effective. Second, for each loop hub, if the candidate is present at all three pools of sgRNA1, sgRNA2 and control, the candidate with peptide counts in both sgRNA1 and sgRNA2 ≥ 2 folds of peptide counts in control is considered as effective. Third, if the candidate is considered as effective in all three loop hubs, it will be included in the final list as the component of β-catenin condensates.

HiChIP data analysis

The clean reads were aligned to the hg19 reference genome using HiC-Pro (v2.11.1) [54]. HiChIP peaks and significant interactions were called using Hichipper (v0.7.7) with the default parameters -min-dist 5000 -max-dist 2,000,000 [55]. All replicates were merged, and all read pairs were used to call peaks. Contacts with FDR ≤ 0.01 and read pairs ≥ 2 were defined as contacts, and the HiChIP peak-related contacts were termed putative interactions.

Definition of loop hubs and hub genes

Chromatin loops identified from HiChIP data are utilized to define loop hubs, crucial for elucidating regulatory relationships within the genome. If two genes respectively overlap

with the two anchors of the same loop, we consider these genes to be linked in proximity, reflecting their spatial closeness. When the total number of genes exceeds ten, we classify these connections as loop hubs. Subsequently, we gather these genes and depict the networks of loop hubs. The overlapping regions between genes and loop anchors are analyzed using bedtools, and the resulting networks are visualized using Cytoscape.

Hi-C data analysis

The public Hi-C data of the CRC and normal colon tissues (GSE133928) were used for loop identification [22]. The Hi-C reads were mapped to the human reference genome (hg19) and allowed the identification of all valid Hi-C interaction pairs using HiC-Pro [54]. The valid pairs were subsequently used to create contact matrices, followed by the application of the Iterative Correction and Eigenvector Decomposition (ICE) method [56] to normalize the matrix. Chromatin loops were identified using peakachu [57] at 5 kb resolution, and a probability threshold of 0.9 for loop calling to ensure high confidence in the identified loops.

Supplementary Information

The online version contains supplementary material available at https://doi.org/10.1186/s13059-026-04030-0.

Additional file 1: Figures S1–S7 and figure legend.

Additional file 2: Table S1. DEGs from RNA-seq between HCT116 and NCM460 cells.

Additional file 3: Table S2. Loop Hubs identified by HiChIP in HCT116 cells, and Hub Genes.

Additional file 4: Table S3. Components of β-catenin Condensates by dCas9-APEX2-MS.

Additional file 5: Table S4. Genome Binding of β-catenin, FUS and DHX9 in HCT116 by ChIP-seq.

Additional file 6: Table S5. H3K4me3 Genome Distribution by CUT&Tag.

Additional file 7: Table S6. RNA-seq data for FUS-deleted, PARP1-deleted, and control HCT116 cells.

Additional file 8: Table S7. Oligonucleotides Information Used in This Study.

Additional file 9: Uncropped images of blot.

Acknowledgements

We thank Huabin Gao (The First Affiliated Hospital, Sun Yat-Sen University, Guangzhou, China) for providing the NCM460 cell line.

Peer review information

Andrew Cosgrove and Wenjing She were the primary editors of this article and managed its editorial process and peer review in collaboration with the rest of the editorial team. The peer-review history is available in the online version of this article.

Authors' contributions

J.Y.Y., H.Y.Z., Y.Y.H.Y., S.S.L., Y.N.L., D.L.T. and X.N.H. performed HiChIP, ChIP-seq, CUT&Tag, RNA-seq and 3C; J.Y.Y., H.Y.Z., Y.Y.H.Y., L.F.Z., Y.X., Y.J.L, Y.J.Z. and J.X.Z. performed phase separation-related experiments; J.Y.Y. and H.Y.Z. cultured the cells and performed perturbation assays; H.Y.Z., J.S., Y.Y.H.Y., W.T.C., J.Y.M. and Y.P. analyzed the raw data; J.W., J.Y.Y, J.S. and H.Y.Z. prepared all figures; J.W., Q.G. and H.Y.Z. wrote the manuscript; all authors reviewed the manuscript; J.W. and Q.G. supervised the work; J.W., H.M.W., J.S. and H.B.G. funded the work. All authors read and approved the final manuscript.

Funding

This research was mainly funded by the National Natural Science Foundation of China (Grant Nos. 32270679 and 32361163609) to J.W., and was also funded by the Guangdong Natural Science Fund, China (Grant No. 2025A1515010534) to Q.G., the National Natural Science Foundation of China (Grant No. 82103084) to H.M.W., the National Natural Science Foundation of China (Grant No. 32400561) to J.S., and the National Natural Science Foundation of China (Grant No. 82403041) to H.B.G.

Data availability

The HiChIP, ChIP-seq, CUT&Tag, RNA-seq data generated in this study have been deposited in the Genome Sequence Archive [58] in National Genomics Data Center [59], China National Center for Bioinformation/Beijing Institute of Genomics, Chinese Academy of Sciences under accession number HRA009167. The data is available at https://ngdc.cncb.ac.cn/gsa-human/browse/HRA009167 [60]. DEGs between HCT116 and NCM460 cells by RNA-seq, loop hubs identified by HiChIP, the components of β-catenin condensate by dCas9-APEX2-MS, genome binding peaks by FUS, DHX9, and

β-catenin ChIP-seq, H3K27ac peaks by CUT&Tag, and RNA-seq data of FUS-deleted, PARP1-deleted, and control HCT116 cells reported in this paper are listed in the Additional file 2: Table S1, Additional file 3: Table S2, Additional file 4: Table S3, Additional file 5: Table S4, Additional file 6: Table S5, and Additional file 7: Table S6, respectively. Hi-C data in normal colon and CRC tissues from Johnstone et al. [22] are accessible in GEO under accession number GSE133928. RNA-seq date of human CRC cell line HCT116 with CTNNB1 WT or knockout genes from Fröhlich et al. [23] are accessible in GEO under accession number GSE199835. RNA-seq date of HCT116 cells treated with CHIR99021 or not from Riley et al. [24] are accessible in GEO under accession number GSE251665. Fluorescence data have been deposited on Figshare with https://doi.org/10.6084/m9.figshare.31028833 [61].

Declarations

Ethics approval and consent to participate

Not applicable as ethical approval was not needed for this study.

Consent for publication

The manuscript is original and has not been published elsewhere or submitted to othe journals. All authors have approved the manuscript for publication.

Competing interests

The authors declare no competing interests.

Author details

[1]GMU-GIBH Joint School of Life Sciences, Guangdong Provincial Key Laboratory of Protein Modification and Disease, The Guangdong-Hong Kong-Macao Joint Laboratory for Cell Fate Regulation and Diseases, Guangzhou Institute of Cancer Research, the Affiliated Cancer Hospital, Guangzhou Medical University, Guangzhou 511436, China. [2]Department of Thoracic Surgery and West China Biomedical Big Data Center, West China Hospital, Sichuan University, Chengdu 610041, China. [3]Med-X Center for Informatics, Sichuan University, Chengdu 610041, China. [4]School of Basic Medical Sciences, Guangzhou Medical University, Guangzhou 511436, China. [5]Zhongshan School of Medicine, Sun Yat-Sen University, Guangzhou 510080, China. [6]Department of General Surgery (Colorectal Surgery), The Sixth Affiliated Hospital, Sun Yat-Sen University, Guangzhou 510655, China. [7]Department of Pathology, the First Affiliated Hospital, Sun Yat-Sen University, Guangzhou 510080, China.

Received: 6 August 2025 Accepted: 5 March 2026
Published online: 19 March 2026

References

1. Bonev B, et al. Multiscale 3D genome rewiring during mouse neural development. Cell. 2017;171(3):557-572 e24.
2. Dall'Agnese A, et al. Transcription factor-directed re-wiring of chromatin architecture for somatic cell nuclear reprogramming toward trans-differentiation. Mol Cell. 2019;76(3):453-472 e8.
3. Krijger PH, et al. Cell-of-Origin-Specific 3D Genome Structure Acquired during Somatic Cell Reprogramming. Cell Stem Cell. 2016;18(5):597–610.
4. Mumbach MR, et al. HiChIP: efficient and sensitive analysis of protein-directed genome architecture. Nat Methods. 2016;13(11):919–22.
5. Fullwood MJ, et al. An oestrogen-receptor-α-bound human chromatin interactome. Nature. 2009;462(7269):58–64.
6. Fang R, et al. Mapping of long-range chromatin interactions by proximity ligation-assisted ChIP-seq. Cell Res. 2016;26(12):1345–8.
7. Flavahan WA, et al. Insulator dysfunction and oncogene activation in IDH mutant gliomas. Nature. 2016;529(7584):110–4.
8. Xu J, et al. Subtype-specific 3d genome alteration in acute myeloid leukaemia. Nature. 2022;611(7935):387–98.
9. Hnisz D, et al. Activation of proto-oncogenes by disruption of chromosome neighborhoods. Science. 2016;351(6280):1454–8.
10. Phanstiel DH, et al. Static and dynamic DNA loops form AP-1-bound activation hubs during macrophage development. Mol Cell. 2017;67(6):1037-1048 e6.
11. Li T, et al. OCEAN-C: mapping hubs of open chromatin interactions across the genome reveals gene regulatory networks. Genome Biol. 2018;19(1):54.
12. Wang J, et al. Phase separation of OCT4 controls TAD reorganization to promote cell fate transitions. Cell Stem Cell. 2021;28(10):1868-1883 e11.
13. Brangwynne CP, et al. Germline P granules are liquid droplets that localize by controlled dissolution/condensation. Science. 2009;324(5935):1729–32.
14. Sabari BR, et al. Coactivator condensation at super-enhancers links phase separation and gene control. Science. 2018. https://doi.org/10.1126/science.aar3958.
15. Boija A, et al. Transcription factors activate genes through the phase-separation capacity of their activation domains. Cell. 2018;175(7):1842-1855 e16.
16. Tatavosian R, et al. Nuclear condensates of the Polycomb protein chromobox 2 (CBX2) assemble through phase separation. J Biol Chem. 2019;294(5):1451–63.
17. Banani SF, et al. Compositional control of phase-separated cellular bodies. Cell. 2016;166(3):651–63.
18. Kilgore HR, Young RA. Learning the chemical grammar of biomolecular condensates. Nat Chem Biol. 2022;18(12):1298–306.

19. Ning W, et al. DrLLPS: a data resource of liquid-liquid phase separation in eukaryotes. Nucleic Acids Res. 2020;48(D1):D288–95.
20. Zamudio AV, et al. Mediator condensates localize signaling factors to key cell identity genes. Mol Cell. 2019;76(5):753-766 e6.
21. Wei C, et al. CTCF organizes inter-A compartment interactions through RYBP-dependent phase separation. Cell Res. 2022;32(8):744–60.
22. Johnstone SE, et al. Large-scale topological changes restrain malignant progression in colorectal cancer. Cell. 2020;182(6):1474-1489 e23.
23. Frohlich J, Rose K, Hecht A. Transcriptional activity mediated by beta-CATENIN and TCF/LEF family members is completely dispensable for survival and propagation of multiple human colorectal cancer cell lines. Sci Rep. 2023;13(1):287.
24. Riley JJ, et al. Widespread 3′ UTR splicing regulates expression of oncogene transcripts through multiple mechanisms. Nucleic Acids Res. 2025. https://doi.org/10.1093/nar/gkaf700.
25. Yeo NC, et al. An enhanced CRISPR repressor for targeted mammalian gene regulation. Nat Methods. 2018;15(8):611–6.
26. Wang J, et al. A molecular grammar governing the driving forces for phase separation of prion-like RNA binding proteins. Cell. 2018;174(3):688-699 e16.
27. Tanenbaum ME, et al. A Protein-Tagging System for Signal Amplification in Gene Expression and Fluorescence Imaging. Cell. 2014;159(3):635–46.
28. Myers SA, et al. Discovery of proteins associated with a predefined genomic locus via dCas9-APEX-mediated proximity labeling. Nat Methods. 2018;15(6):437–9.
29. Sun J, et al. Precise prediction of phase-separation key residues by machine learning. Nat Commun. 2024. https://doi.org/10.1038/s41467-024-46901-9.
30. Chen Z, et al. Screening membraneless organelle participants with machine-learning models that integrate multimodal features. Proc Natl Acad Sci U S A. 2022;119(24):e2115369119.
31. Alanis-Lobato G, Andrade-Navarro MA, Schaefer MH. HIPPIE v2.0: enhancing meaningfulness and reliability of protein-protein interaction networks. Nucleic Acids Res. 2017;45(D1):D408–14.
32. Hnisz D, et al. A phase separation model for transcriptional control. Cell. 2017;169(1):13–23.
33. Karpinska MA, et al. Ctcf depletion decouples enhancer-mediated gene activation from chromatin hub formation. Nat Struct Mol Biol. 2025. https://doi.org/10.1038/s41594-025-01555-z.
34. Gambi G, et al. 3D chromatin hubs as regulatory units of identity and survival in human acute leukemia. Mol Cell. 2025;85(1):42-60 e7.
35. Han TW, et al. Cell-free formation of RNA granules: bound RNAs identify features and components of cellular assemblies. Cell. 2012;149(4):768–79.
36. Kato M, et al. Cell-free formation of RNA granules: low complexity sequence domains form dynamic fibers within hydrogels. Cell. 2012;149(4):753–67.
37. Qamar S, et al. FUS phase separation is modulated by a molecular chaperone and methylation of arginine cation-pi interactions. Cell. 2018;173(3):720-734 e15.
38. Hofweber M, et al. Phase separation of FUS is suppressed by its nuclear import receptor and arginine methylation. Cell. 2018;173(3):706-719 e13.
39. Mitrea DM, et al. Modulating biomolecular condensates: a novel approach to drug discovery. Nat Rev Drug Discov. 2022;21(11):841–62.
40. Krishnakumar R, Kraus WL. PARP-1 regulates chromatin structure and transcription through a KDM5B-dependent pathway. Mol Cell. 2010;39(5):736–49.
41. Gao H, et al. Phase separation of DDX21 promotes colorectal cancer metastasis via MCM5-dependent EMT pathway. Oncogene. 2023;42(21):1704–15.
42. Hagège H, et al. Quantitative analysis of chromosome conformation capture assays (3C-qPCR). Nat Protoc. 2007;2(7):1722–33.
43. Kaya-Okur HS, et al. CUT&tag for efficient epigenomic profiling of small samples and single cells. Nat Commun. 2019. https://doi.org/10.1038/s41467-019-09982-5.
44. Lu B, et al. Phase separation of phospho-HDAC6 drives aberrant chromatin architecture in triple-negative breast cancer. Nat Cancer. 2024. https://doi.org/10.1038/s43018-024-00816-y.
45. Chen S, et al. Fastp: an ultra-fast all-in-one FASTQ preprocessor. Bioinformatics. 2018;34(17):i884–90.
46. Langmead B, Salzberg SL. Fast gapped-read alignment with Bowtie 2. Nat Methods. 2012;9(4):357-U54.
47. Li H, et al. The sequence alignment/map format and SAMtools. Bioinformatics. 2009;25(16):2078–9.
48. Zhang Y, et al. Model-based analysis of ChIP-Seq (MACS). Genome Biol. 2008. https://doi.org/10.1186/gb-2008-9-9-r137.
49. Quinlan AR, Hall IM. BEDTools: a flexible suite of utilities for comparing genomic features. Bioinformatics. 2010;26(6):841–2.
50. Anders S, Pyl PT, Huber W. Htseq-a python framework to work with high-throughput sequencing data. Bioinformatics. 2015;31(2):166–9.
51. Robinson MD, McCarthy DJ, Smyth GK. edgeR: a Bioconductor package for differential expression analysis of digital gene expression data. Bioinformatics. 2010;26(1):139–40.
52. Wang J, et al. YY1 positively regulates transcription by targeting promoters and super-enhancers through the BAF complex in embryonic stem cells. Stem Cell Reports. 2018;10(4):1324–39.
53. Ding J, et al. Oct4 links multiple epigenetic pathways to the pluripotency network. Cell Res. 2012;22(1):155–67.
54. Servant N, et al. HiC-Pro: an optimized and flexible pipeline for Hi-C data processing. Genome Biol. 2015. https://doi.org/10.1186/s13059-015-0831-x.
55. Lareau CA, Aryee MJ. Hichipper: a preprocessing pipeline for calling DNA loops from HiChIP data. Nat Methods. 2018;15(3):155–6.

56. Imakaev M, et al. Iterative correction of Hi-C data reveals hallmarks of chromosome organization. Nat Methods. 2012;9(10):999–1003.
57. Salameh TJ, et al. A supervised learning framework for chromatin loop detection in genome-wide contact maps. Nat Commun. 2020. https://doi.org/10.1038/s41467-020-17239-9.
58. Chen T, et al. The genome sequence archive family: toward explosive data growth and diverse data types. Genomics Proteomics Bioinformatics. 2021;19(4):578–83.
59. Members CN, Partners. Database resources of the National Genomics Data Center, China National Center for Bioinformation in 2022. Nucleic Acids Res. 2022;50(D1):D27–38.
60. Yang J, Sun J, Zhang H, Yu Y, Chen F, Mo J, Luo S, Xu Y, Zhong L, Tan D, Lin Y, Liao Y, Zhang Y, Zhang J, Chen W, Huang X, Peng Y, Gao H, Wang H, Gong Q, Wang J. HiChIP, ChIP-seq, CUT&Tag, RNA-seq data. Genome Sequence Arch. PRJCA030890. 2025. https://ngdc.cncb.ac.cn/gsa-human/browse/HRA009167.
61. Yang J, Sun J, Zhang H, Yu Y, Chen F, Mo J, et al. Fluorescence data. 2026. Figshare. https://doi.org/10.6084/m9.figshare.31028833.

Publisher's Note